Copyright Warning & Restrictions

The copyright law of the United States (Title 17, United States Code) governs the making of photocopies or other reproductions of copyrighted material.

Under certain conditions specified in the law, libraries and archives are authorized to furnish a photocopy or other reproduction. One of these specified conditions is that the photocopy or reproduction is not to be "used for any purpose other than private study, scholarship, or research." If a, user makes a request for, or later uses, a photocopy or reproduction for purposes in excess of "fair use" that user may be liable for copyright infringement,

This institution reserves the right to refuse to accept a copying order if, in its judgment, fulfillment of the order would involve violation of copyright law.

Please Note: The author retains the copyright while the New Jersey Institute of Technology reserves the right to distribute this thesis or dissertation

Printing note: If you do not wish to print this page, then select "Pages from: first page # to: last page #" on the print dialog screen

ABSTRACT

NARROW-BAND INTERFERENCE REJECTION IN SPREAD SPECTRUM USING AN EIGENANALYSIS BASED APPROACH

by
Aparna Vadhri

A new adaptive technique is suggested for rejecting narrow-band interferences in spread spectrum communications. When data is coded using a pseudo-noise code, the received signal consists of a wide-band signal with almost white spectral properties, thermal noise, and correlated narrow-band interferences. A new approach is proposed which exploits the statistical properties of the received signal via eigenanalysis of the received data. While the energy of the wide-band signal is distributed over all the eigenvalues of the signal autocorrelation matrix, the energy of the interference is concentrated in a few large eigenvalues. Hence, the eigenvectors corresponding to the large eigenvalues are termed the *interference subspace*. The proposed method derives a weight vector residing in the subspace spanned by the rest of the eigenvectors termed the *noise subspace*. Consequently, it is orthogonal to the interference subspace. The eigenanalysis based interference cancellation is sub-optimal in a known signal environment, but is superior to the Wiener-Hopf filter when the signal statistics are estimated from a limited amount of data. A fast and effective adaptive algorithm is derived using the power method.

NARROW-BAND INTERFERENCE REJECTION IN SPREAD SPECTRUM USING AN EIGENANALYSIS BASED APPROACH

by
Aparna Vadhri

A Thesis
Submitted to the Faculty of
New Jersey Institute of Technology
in Partial Fulfillment of the Requirements for the Degree of
Master of Science in Electrical Engineering

Department of Electrical and Computer Engineering

May 1994

APPROVAL PAGE

NARROW-BAND INTERFERENCE REJECTION IN SPREAD SPECTRUM USING AN EIGENANALYSIS BASED APPROACH

Aparna Vadhri

Dr. Alexander Haimovich, Thesis Advisor / Date
Associate Professor of Electrical and Computer Engineering,
NJIT

Dr. Nirwan Ansari, Committee Member / Date
Associate Professor of Electrical and Computer Engineering,
NJIT

Dr. Zoran Siveski, Committee Member Date
Assistant Professor of Electrical and Computer Engineering,
NJIT

BIOGRAPHICAL SKETCH

Author: Aparna Vadhri

Degree: Master of Science in Electrical Engineering

Date: May 1994

Undergraduate and Graduate Education:

- Master of Science in Electrical Engineering,
  New Jersey Institute of Technology, Newark, NJ, 1994

- Bachelor of Science in Electrical Engineering,
  Lafayette College, Easton, PA, 1992

Major: Electrical Engineering

Presentations and Publications:

A. Haimovich and A. Vadhri, "Rejection of Narrow-Band Interferences in PN Spread Spectrum Systems Using an Eigenanalysis Algorithm," to be presented at *IEEE Statistical Signal Processing Workshop*, June 1994

A. Haimovich and A. Vadhri, "Rejection of Narrow-Band Interferences in PN Spread Spectrum Systems Using an Eigenanalysis Approach," to be presented at *MILCOM*, October 1994

Of the four lions on Ashoka's capitol
three are visible whereas the fourth one is not.
In a student's life, there are three forces
recognized to ascertain her/his degree of success in academia:
the student who imbibes learning,
the teacher who imparts knowledge,
and the father whose name the student carries.
However, very often, it is the mother who is not recognized
for her Herculean efforts; hence, the fourth invisible lion.
This work is dedicated to my parents,
V.V.S. Subba Rao and V.S. Sarada, the fourth lion

ACKNOWLEDGMENT

This work would not have been possible if it were not for Dr. Alexander Haimovich whose guidance and support throughout the research culminated in this work. I especially appreciate his role as a mentor and advisor. His keen insight helped shape not only my work but also my approach toward research in engineering. Special thanks are also due to Drs. Nirwan Ansari and Zoran Siveski for their advice and support as well.

Among my colleagues, I wish to recognize Dr. Raafat Kamel for his patient review of my thesis, especially for his perspicacity in my presentation of the material. Mr. Chris Peckham, who went way beyond his scope of duties as a system administrator, and Dr. Ruth Onn rescued me from many frustrating moments with the Sun Workstations. Ms. Xiao Cheng (Susan) Wu helped with various facets of the theory behind this work. I also wish to recognize Mr. Andrew Bateman for his help in ironing out many details of the thesis. Thanks to Ms. Lisa Fitton who reviewed my thesis and helped with many other day-to-day details in the lab. I appreciate all of my colleagues in the lab, especially Ms. Zebiba Shifa, for their friendship and support which helped alleviate the stressful moments during the research.

Mr. Ross Bettinger, of Lincoln Labs, provided valuable material which helped in my research.

Finally, I wish to thank my parents and my sister for their love and support, which needless to say, kept me going through all these years.

TABLE OF CONTENTS

LIST OF TABLES

LIST OF FIGURES

CHAPTER 1

INTRODUCTION

Spread spectrum systems are widely employed as signal modulators and transmitters in the military and mobile communications fields. Their payoffs are many; most notably, interference rejection, multipath suppression, low probability of interception, and random accessing by multiple users. Of these, the single most important inherent aspect of spread spectrum systems is interference rejection [21]. This work focuses on the rejection of narrow-band interferences in spread spectrum systems.

The spread spectrum system spreads a data signal over a much wider bandwidth than necessary to transmit the information. This, in turn, translates into a *processing gain*, so called because the signal achieves a gain in power over the interference during processing. Of the various spreading techniques, the direct-sequence (DS) system is considered in this work. In a DS system, each data bit is modulated by a pseudorandom or pseudonoise (PN) code. The resulting short pulses, called chips, form a sequence with white power spectral density. The wide-band data is then transmitted.

The data is received at the destination, corrupted by thermal noise, commonly modeled as an additive white Gaussian noise. In addition to thermal noise, other interferences, both narrow-band and comparable in bandwidth to the spread spectrum bandwidth, may co-exist in the same portion of the frequency spectrum as the modulated signal. The degree of distortion caused in the received signal is proportional to the portion of the signal bandwidth the interferences occupy as well as their power. It is well known that the matched filter is the optimal processor for a known signal, in our case, the interferences, in white Gaussian noise. The received signal is subsequently demodulated, using the same PN code that was used to modulate the desired signal in the first place. The interference is

effectively decorrelated and assumes a white noise-like appearance. Consequently, the interference bandwidth is spread out over the entire spread spectrum system bandwidth, thereby mitigating the effect of the interference power throughout the spread spectrum bandwidth. Summing the output of the PN demodulator over the data bit time interval restores the original data and averages out the noise-like interference, thereby removing the interference outside the signal bandwidth. In the process, the bandwidth of the desired signal collapses to the original data bandwidth. Consequently, only a fraction of the interference power, namely the ratio of the spread spectrum bandwidth over the signal bandwidth termed as the *compression ratio*, serves to distort the desired signal. This is the matched filter, optimal for a known signal in white Gaussian noise, but effective against interference to the extent of the processing gain [10].

The spread spectrum system is inherently as effective in combating the wide-band interferences as it is capable of handling the narrow-band interferences. In other words, the system rejects a wide-band interference of a certain power with the same effectiveness as it rejects a narrow-band interference of the same power. This is because the improvement in the signal-to-interference ratio (SIR) termed as the *processing gain* is equal to the compression ratio. Therefore, the processing gain of a spread spectrum receiver is *independent* of the interference bandwidth and power. Likewise, the resulting SIR at the output of the filter is independent of the interference bandwidth; however, it is dependent upon the power of the interference.

When the power of the interference is so great that the increase in SIR due to the processing gain of the fixed matched filter is not satisfactory, it is necessary to use a matched filter for the noise *and* the interference. This work addresses the rejection of narrow-band interferences. Hence, the matched filter is implemented by processing the received signal through a narrow-band filter before demodulation. The narrow-band filter is designed to notch the interference out. As a result, the frequency

components of the desired signal that occupy the same region as the interference are notched out as well. This distortion is negligible if the interference bandwidth is small compared to the spread spectrum bandwidth.

If the interference power spectral density is fixed and known, then an optimal filter can be designed that estimates and removes the narrow-band interference from the data with minimum mean square error (MSE). The optimal filter is also known as the Wiener-Hopf filter. It is optimal because it operates under the assumption that the interference statistics are known and accordingly minimizes the power of the interference, given by the mean square (MS) at the output of the interference-suppressant filter. The optimal filter calculates and removes the correlated portion of the received signal. Since the received signal consists of the wide-band spread spectrum signal, thermal noise, and the narrow-band interference, the correlation is mainly due to the interference.

If the interference power spectral density, or equivalently, the correlation function, is not known, it can be estimated from the data. For a stationary environment, the estimate improves as the size of the data record is increased. When the interference cannot be represented by a stationary process, a recursive algorithm is required to update the coefficients of the optimal filter. Several recursive algorithms based on the Wiener-Hopf filter have been developed.

One class of such algorithms is the Widrow-Hoff least mean squared (LMS). Widrow, *et al.* [25] provided an extensive review of the performance of the Widrow-Hoff LMS algorithm implemented using a digital filter for the purpose of array processing. Compton [1] first introduced the Widrow LMS implemented in an adaptive filter in PN spread spectrum systems for the purpose of nulling the interference. Iltis and Milstein [13] furthered the work in [1] by providing extensive analysis of the performance of the Widrow LMS algorithm implemented in a linear transversal filter in PN spread spectrum systems.

Another class of algorithms is based on minimizing the least-squares (LS) criterion. One particular member of this class developed by Godard [4] is the recursive least squares (RLS). Eleftheriou and Falconer [3] provided analysis of the performance of the RLS implemented in an adaptive filter to rapidly track an unknown signal. Another member of this class of LS-based algorithms is the linear least squares estimation (LLSE) algorithm. Iltis and Milstein [12] considered the application of the LLSE algorithm in DS spread spectrum systems to excise narrow-band interference. Milstein and Iltis [20] and Milstein [19] provided overviews of several of the popular algorithms implemented in linear transversal filters for excision of narrow-band interference in PN spread spectrum, including LMS and LLSE techniques.

Both the LMS and the RLS algorithms are widely used in tracking signals in unknown environments. Therefore, they have been implemented in digital filters to estimate and cancel narrow-band interferences in spread spectrum. Hsu and Giordano [11] first used *digital whitening* filters in the form of *linear prediction* filters in PN spread spectrum systems to excise correlated portions of a signal, namely the interference, in a white Gaussian environment. Gaussian statistics were assumed to maintain the linearity of the filter.

Ketchum and Proakis [15] provided extensive expressions for the performance of linear prediction filters in terms of the signal-to-noise-and-interference (SNIR) ratio and the probability of error, assuming Gaussian statistics given narrow-band interferences. Li and Milstein [16] provided closed-form analytic expressions for the performance of linear transversal filters in the presence of a tone interference in a white Gaussian environment. Masry [17] extended all work previously done in the area of narrow-band interference rejection in PN spread spectrum systems using linear prediction filters. He provided closed-form analytic expressions for the performance of such filters in various narrow-band interference environments,

including both deterministic and non-deterministic interferences. He further extended the work in [15] by providing *exact* closed form analytic expressions for the performance of linear prediction filters based on their length. Furthermore, he wrote an extended paper offering exact closed form analytic expressions for the performance of linear *interpolation* filters in PN spread spectrum systems [18]. However, this work will deal exclusively with linear prediction filters.

As noted before, the Wiener-Hopf and the Wiener-based algorithms estimate and cancel the interference by exploiting the correlation properties of the received signal. This work presents a new method and algorithm which exploit the eigen-properties of the autocorrelation matrix of the received signal. It belongs to a class termed *eigenfilters* because these filters take advantage of the eigen-structure of the autocorrelation matrix of the received signal as opposed to other filters which examine the correlation properties of the signal. These eigenfilters have been implemented in adaptive array processing, e.g., as spectral estimators used to resolve spatially distributed signals [2]. An eigenfilter has also been proposed to separate the *desired signal sources* from *background noise* by resolving them into their respective eigen-vector subspaces of the signal eigen-space. By designating the narrow-band interferences as the *desired signal sources*, they are cancelled if a weight vector of the adaptive filter is placed in an eigen-subspace orthogonal to the interference [6].

This work seeks to implement this eigenfilter in DS spread spectrum systems, to take advantage of the *noise-like* appearance of the modulated wide-band signal, to resolve the correlated interference and the modulated signal and uncorrelated thermal noise into two mutually orthogonal eigen-subspaces. Hence, the modulated data and thermal noise are designated as the *background noise* sources. Then, a weight vector could be created residing in the noise subspace that would excise the interference while preserving most of the data.

The autocorrelation matrix can be represented in terms of its eigenvalues and their respective eigenvectors. Both the modulated signal and thermal noise are modeled as white processes, distributing the energy evenly over the eigenvalues of the received data correlation matrix. Conversely, the energy of the narrow-band interference is concentrated in only a few large eigenvalues. The eigenvectors associated with those eigenvalues span a subspace of the signal eigen-space termed the *interference subspace*. The rest of the eigenvectors span the *noise subspace*, so called because most of the white noise resides here. Since the eigenvectors of an autocorrelation matrix are mutually orthogonal, the interference subspace is orthogonal to the noise subspace.

If the adaptive tap-weights of the filter are chosen in the noise subspace, they are orthogonal to the interference subspace. Therefore, passing the received signal through this filter preserves most of the signal and noise while effectively canceling the interference; hence, this eigenanalysis based method is called an *Eigencanceler* [6].

The Eigencanceler differs from the Wiener-Hopf in two fundamental ways:

1. Its design is *not* based on minimizing both the noise *and* the interference power at the output of the filter. It handles both signals separately.

2. It has a constraint that its tap-weight vector resides in an eigen-subspace which is orthogonal to the interference subspace.

As stated previously, the Wiener-Hopf filter is the optimal interference canceller in a known signal environment. As such, the Eigencanceler is sub-optimal to the Wiener-Hopf under these conditions. In practical situations, however, the signal statistics are unknown and must be estimated, resulting in varying estimates of the eigenvalues and eigenvectors of the time-estimated autocorrelation matrix. The insensitivity to the inverse of the small, but fluctuating, noise eigenvalues allows the Eigencanceler

to deliver superior interference cancellation over the Wiener-Hopf given a relatively small batch of signal samples whose correlation properties are unknown. This is because the size of the data directly reflects on the measurement noise perturbation over the estimation of the interference. Measurement noise perturbation results from the estimation of the correlation statistics of the recieved signal, which vary from sample to sample of the incoming signal. The smaller the batch of signal samples, the more perturbation there exists. Also, the lower the interference power is, the greater the perturbation by the measurement noise, since the harder it is to detect the interference. Under such circumstances, the Eigencanceler will offer superior interference cancellation over the Wiener-Hopf, while extracting the desired signal with a relatively high degree of fidelity.

Where the interference cannot be represented by stationary processes, recursive algorithms are developed to update the weight vector of the filter at every incoming signal sample. Practical implementations of the Wiener-Hopf are formed in the aforementioned recursive algorithms. The insensitivity of the Eigencanceler to the measurement noise allows for fast convergence to its optimal solution, as opposed to the Wiener-based algorithms, which are perturbed, in varying degrees, by the measurement noise. The usefulness of the Eigencanceler is therefore evident, especially when given highly non-stationary interferences. Such an environment would require that an interference-suppressant filter be able to adapt within a few iterations to suppress a significant portion of the interference successfully. Consequently, one can build a fast-tracking adaptive filter based on the Eigencanceler and suppress the interference effectively.

The Eigencanceler approach proposed in this work will be developed with a *block method* and a *recursive algorithm.* The former is known as a block method, because data is collected over a period of time in a block format. The block of data yields the autocorrelation matrix which is subsequently subjected to eigenanalysis in

order to develop the Eigencanceler. The latter is a recursive algorithm, developed via the classical *power method* designed to derive the eigenvector(s) corresponding to the largest eigenvalues from the estimate of the autocorrelation matrix of the received signal [5].

The scope of this work is to test the algorithm based on the Eigencanceler against a good sample representative of the other existing algorithms used for the signal environment presented in this work. Two of the aforementioned Wiener-based algorithms, namely, the LMS and the RLS, will be used in this work. The algorithms are briefly introduced here:

1. The LMS is simple to implement, i.e., it does not store the past data samples, only the updated filter tap weights, and it does not require matrix inversion [22]. The LMS attempts to minimize the MSE, with the error defined as the difference between the current sample of the signal and the output of the filter [24]. The error is used in the updating process of the filter tap weights to reduce the MSE with each successive iteration. Due to gradient noise, the LMS is said to converge to the Wiener solution in the mean. However, the main drawback of the LMS is its sensitivity to the eigenvalue spread. In an environment where the eigenvalue spread of the autocorrelation matrix of the received signal is greater than ten decibels (dB), it is well known that the convergence rate of the LMS slows down significantly, i.e., the LMS is highly sensitive to the eigenvalue spread [10].

2. The RLS algorithm is less sensitive to the eigenvalue spread than the LMS, given a high SNR, and it is known to produce zero excess mean squared error (MSE) in a stationary environment [10]. However, its chief drawback is its complexity.

The parameters of the problem–the signal model, the receiver, the Wiener-Hopf filter, and the LMS and the RLS algorithms–will be discussed in Chapter 2. The derivation of the Eigencanceler will be covered in Chapter 3. Chapter 4 will focus on the Eigencanceler algorithm. Simulation results based upon figures of merit derived in Chapters 3 and 4 are presented in Chapter 5. The conclusion and discussion of possible future work will be covered in Chapter 6.

CHAPTER 2

THE SYSTEM

This chapter considers the following topics:

1. The signal model, i.e., the generation of the received signal and its statistical properties;
2. The workings of the receiver;
3. The optimal receiver;
4. The adaptive algorithms for the suppression of narrow-band interferences in a spread spectrum environment.

2.1 The Signal Model

The signal model consists of the data signal, the interference, and the thermal noise. Consider a data sequence, with each bit of duration T seconds. Assume bi-polar signalling so the data takes on values [-1,+1]. This signal is passed through a PN modulator serially, where each bit is modulated by a PN code, as depicted in Figure 2.1.

The modulator generates $L = \frac{T}{T_c}$ chips per data bit, where T_c is the duration of each chip. Assume bi-polar signalling so the PN code takes on values [-1,+1], with equal probability, and has white spectral properties. Consequently, the modulated data signal is spread in frequency over the entire spread spectrum bandwidth. Let d_i be the i-th data bit, and let $c(kT_c)$ be the k-th chip in the PN code. Then the modulated data signal u_d is given by:

$$u_{d,i}(kT_c) = d_i c(kT_c),\ k = 1 \ldots L.$$

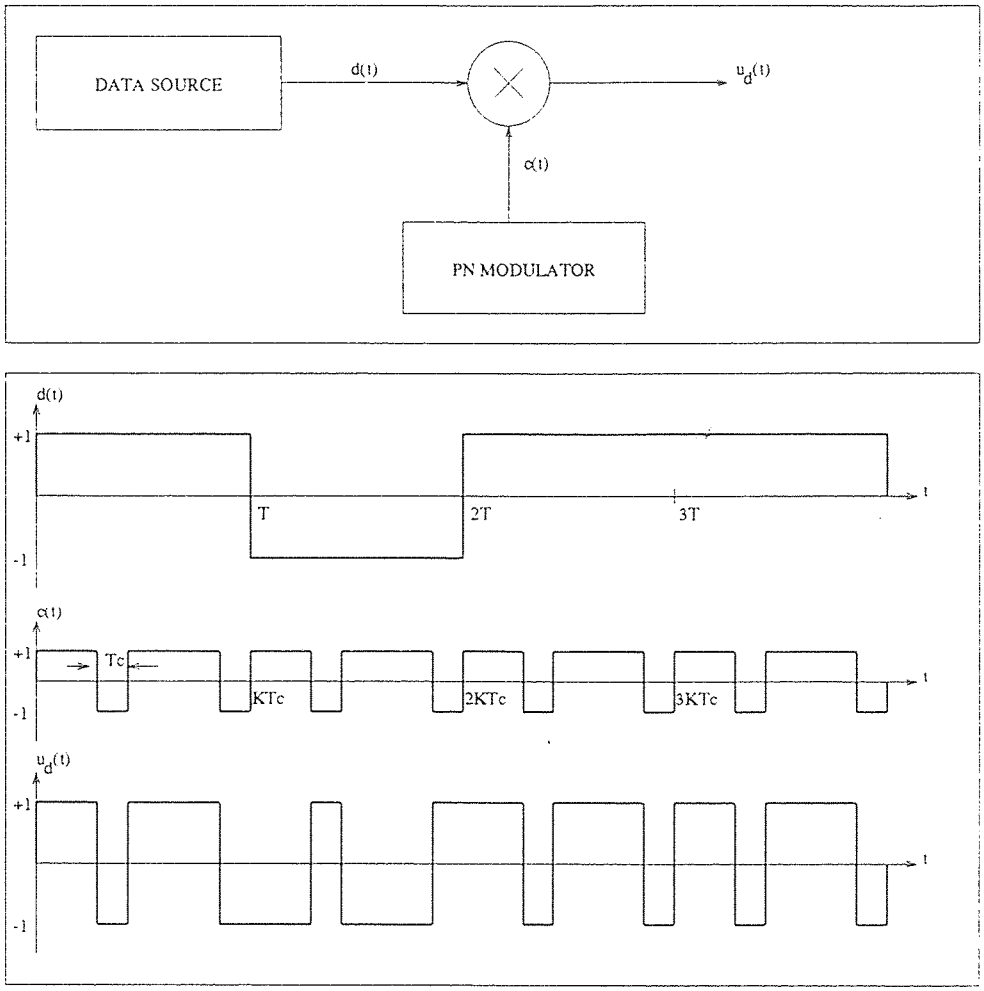

Figure 2.1 The signal model
(a) The transmitter (b) The modulation of the data signal.

For the sake of simplicity, the data has zero-mean and unity variance. Likewise, the PN code too has zero-mean and variance 1. Therefore, the modulated data signal u_d has zero-mean and variance $\sigma_d^2 = 1$.

The modulated signal is corrupted by additive white Gaussian noise and a narrow-band interference. More specifically, two types of narrow-band interference are considered: a *tone interference* and a *narrow-band Gaussian interference.* The former is a sinusoidal signal with *zero* bandwidth, and the latter is a signal, whose bandwidth is narrow with respect to the spread spectrum bandwidth. The inter-

ference tone is modeled by samples of a cosine signal of frequency ω, power J, and random phase θ, which is uniformly distributed in the interval $(0, 2\pi)$. Samples of the interference tone at the chip interval are then given by:

$$u_j(kT_c) = \sqrt{2J}\cos(\omega kT_c + \theta).$$

The autocorrelation matrix of a narrow-band Gaussian interference is given by:

$$\mathcal{R}_j(kT_c) = J\frac{\sin(w_j kT_c/2)}{w_j kT_c/2}\cos(wkT_c)$$

where J and w_j are the power and the bandwidth of the interference, respectively.

The thermal noise is modeled by random signals with Gaussian distribution with a spectral density of σ_n^2.

Therefore, the received signal is given by:

$$\begin{aligned} u_i(kT_c) &= u_{d,i}(kT_c) + u_j(kT_c) + u_n(kT_c),\ k = 1, \ldots, L \\ &= d_i c(kT_c) + u_j(kT_c) + n_k. \end{aligned} \tag{2.1}$$

The data signal and the thermal noise have white spectra, whereas the tone and narrow-band Gaussian interferences are highly correlated. A brief derivation of their autocorrelation functions will demonstrate the degree of correlation for each of the signals. Since the three signals are mutually independent and the PN modulated data signal and thermal noise are white, all of the cross-correlation terms equal zero. Therefore, the ensemble-averaged autocorrelation sequence of the received signal is given by:

$$\mathrm{E}[u_i^2] = \mathrm{E}[u_{d,i}^2] + \mathrm{E}[u_{j,i}^2] + \mathrm{E}[u_{n,i}^2]$$

where

$$\mathrm{E}[u_{dk}u_{dl}] = \begin{cases} 1 & \mathrm{k} = \mathrm{l} \\ 0 & k \neq l \end{cases}$$

$$\mathrm{E}[u_{jk}u_{jl}] = \begin{cases} J\cos\omega(k-l)T_c & \text{for a tone interference} \\ J\frac{\sin w_j(k-l)T_c/2}{w_j(k-l)T_c/2}\cos\omega(k-l)T_c & \text{for a narrow-band interference} \end{cases}$$

$$\mathrm{E}[n_k n_l] = \begin{cases} \sigma_n^2 & \mathrm{k} = \mathrm{l} \\ 0 & \mathrm{k} \neq \mathrm{l}. \end{cases}$$

The autocorrelation sequence of the received signal y is given by:

$$r = \begin{cases} [1 + J + \sigma_n^2,\ J\cos\omega T_c,\ J\cos 2\omega T_c,\ \ldots] & \text{for a tone interference} \\ \left[1 + J + \sigma_n^2,\ J\frac{\sin\omega_j T_c/2}{\omega_j T_c/2}\cos\omega T_c,\ J\frac{\sin 2\omega_j T_c/2}{2\omega_j T_c/2}\cos 2\omega T_c,\ \ldots\right] & \text{for a narrow-band} \\ & \text{interference.} \end{cases}$$

The ensemble-averaged autocorrelation matrix is given by the Toeplitz matrix generated using the ensemble-averaged autocorrelation sequence, consequently, it is represented by:

$$\mathcal{R} = \begin{pmatrix} 1 + J + \sigma_n^2 & J\cos\omega T_c & \ldots & J\cos(M-1)\omega T_c \\ J\cos\omega T_c & 1 + J + \sigma_n^2 & \ldots & J\cos(M-2)\omega T_c \\ \vdots & \vdots & \vdots & \vdots \\ J\cos(M-1)\omega T_c & J\cos(M-2)\omega T_c & \ldots & 1 + J + \sigma_n^2 \end{pmatrix} \tag{2.2}$$

for a tone interference, where M is the length of the filter at the receiver; hence, at any given time, the current sample of the received signal and $M-1$ past samples are stored in the filter.

Likewise, the ensemble-averaged autocorrelation of the received signal for the case of a narrow-band Gaussian interference is

$$\mathcal{R} = \begin{pmatrix} 1 + J + \sigma_n^2 & \ldots & J\frac{\sin(M-1)\omega_j T_c/2}{(M-1)\omega_j T_c/2}\cos(M-1)\omega T_c \\ J\frac{\sin\omega_j T_c/2}{\omega_j T_c/2}\cos\omega T_c & \ldots & J\frac{\sin(M-2)\omega_j T_c/2}{(M-2)\omega_j T_c/2}\cos(M-2)\omega T_c \\ \vdots & \vdots & \vdots \\ J\frac{\sin(M-1)\omega_j T_c/2}{(M-1)\omega_j T_c/2}\cos(M-1)\omega T_c & \ldots & 1 + J + \sigma_n^2 \end{pmatrix}. \tag{2.3}$$

It is noted that the signal and thermal noise terms, namely u_d and u_n, are located on the main diagonal, whereas the interference terms occupy every slot in the matrix.

Now that all the statistical properties of the transmitted and received signals have been covered, the next step is to develop the receiver where the signal is processed.

2.2 The Receiver

The received signal consists of the modulated desired signal, the thermal noise, and the interference. The fixed matched filter will disperse the interference throughout

the spread spectrum system bandwidth. Note that the fixed matched filter delivers the same system performance, i.e., increase in SIR, for an interference of a fixed power, regardless of bandwidth size, as it operates independently from the bandwidth of the interference. Therefore, the filter is sensitive to the interference power, not the interference bandwidth.

As noted previously, sometimes the fixed matched filter will offer a processing gain to the signal such that the output SIR is significantly positive. In other circumstances, however, the processing gain offered by the fixed matched filter may not counter a significantly negative SIR. Consequently, an adaptive filter may be implemented before the PN demodulator to remove the interference from the signal, the drawback being that some of the data signal is distorted. The output of the interference-suppressant filter is passed through the demodulator, whereby the residual interference is spread over the spread spectrum system bandwidth.

The system performance of the adaptive filter is sensitive to both the interference power and bandwidth because the filter notches out the interference estimate. The more power the interference has, the deeper the notch. The more spread spectrum bandwidth the interference occupies, the wider the notch in the region. As a result, the data signal is distorted even further, because the portion of the data signal that occupies the same frequency bandwidth occupied by the interference is notched out along with the interference. One way to compensate for this is to add more tap weights in the adaptive filter so as to increase the accuracy in the estimation of the interference. Another way is to increase the compression ratio, i.e., the number of PN code chips per data bit so that the interference bandwidth occupies a lesser portion of the spread spectrum bandwidth.

In summary, two types of receivers will be discussed: the fixed matched filter receiver and the receiver consisting of the adaptive interference-suppressant filter and

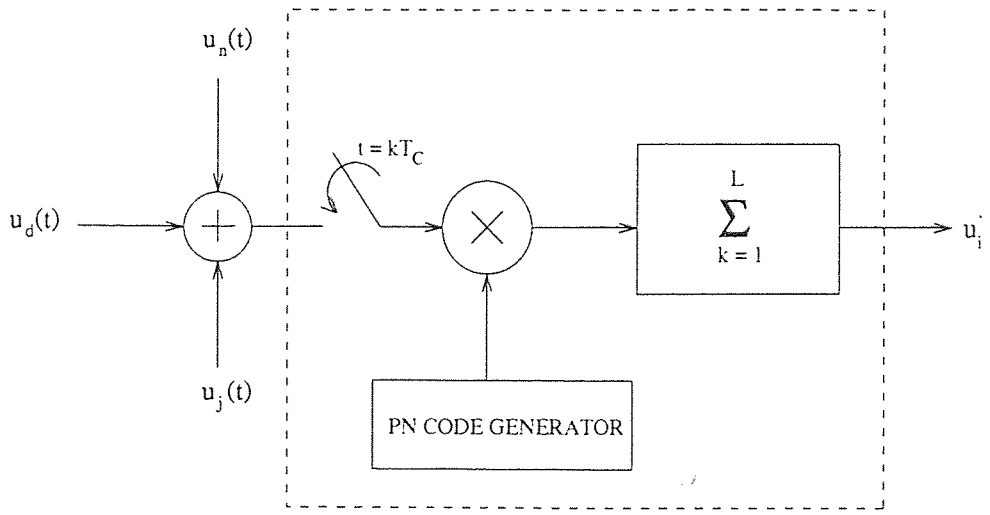

Figure 2.2 The fixed matched filter receiver.

the PN demodulator. Both types of receivers will be evaluated in improvement in SNIR and probability of error.

2.2.1 The Fixed Matched Filter

The filter, depicted in Figure 2.2, consists of a PN code generator, matched to the one at the transmitter, which demodulates the received signal so that the desired signal is restored.

The received signal is given by Equation 2.1:

$$u_i(kT_c) = d_i c(kT_c) + u_j(kT_c) + n_k.$$

The signal is fed into the demodulator and summed over the number of PN code chips per data bit, L chips at a time, yielding the output signal:

$$\begin{aligned} u_i^{'} &= \sum_{k=1}^{L} u_i(kT_c)c(kT_c) \\ &= \sum_{k=1}^{L} [d_i c(kT_c) + u_j(kT_c) + n_k]c(kT_c) \\ &= \sum_{k=1}^{L} d_i c(kT_c)^2 + \sum_{k=1}^{L} c(kT_c)u_j(kT_c) + \sum_{k=1}^{L} c(kT_c)n_k \\ &= Ld_i + u_{j,i}^{'} + n_i^{'}. \end{aligned}$$

The result is the restoration of the original data signal, an interference spread in frequency over the spread spectrum bandwidth, and thermal noise, each with a processing gain of L. The summation acts as a low-pass filter, thereby leaving the data signal intact. However, the portions of the thermal noise and whitened interference lying outside the bandpass filter bandwidth are effectively removed. The ratio of the spread spectrum bandwidth B_{ss} to that of the data B_T is given by:

$$\frac{B_{ss}}{B_T} = \frac{T}{T_c} = L.$$

Since the interference is spread in frequency over the entire spread spectrum bandwidth, the interference effect on the data signal is reduced by a factor of L, because the effective interference lies only within the original data signal bandwidth. Therefore, although the total power of the interference after demodulation is incremented by L, the effective power of the interference on the data signal is marked down by a factor of L. The thermal noise is equally adversely affected by L. The power of the data signal after demodulation is incremented by a factor of L; thus, the SNIR is increased by a factor of L.

To compute the SNIR of a particular bit at the output of the PN demodulator in an adaptive interference-suppressant filter, the mean and the variance of the bit must be computed. Assumptions are made to the effect that the PN sequence is white, the interference has zero-mean with an autocorrelation sequence $\rho_j(k)$, and the thermal noise has white spectral properties with variance σ_n^2. Given these assumptions, the following equation defines the SNIR at the output of the fixed matched filter SNIR_f corresponding to the i-th data bit to be the square of its mean over its variance [15]:

$$\begin{aligned}
\mathrm{SNIR}_f &= \frac{\mathrm{E}^2[u_i']}{\mathrm{E}[|u_i' - \mathrm{E}[|u_i'|]|^2]} \\
&= \frac{\mathrm{E}^2[Ld_i + u_{j,i}' + n_i']}{\mathrm{E}[|Ld_i + u_j(j,i)' + n_i' - \mathrm{E}[Ld_i + u_{j,i}' + n_i']|^2]} \\
&= \frac{L^2 d_i^2}{\mathrm{E}[|u_{j,i}'|^2] + \mathrm{E}[|n_i'|^2]}
\end{aligned}$$

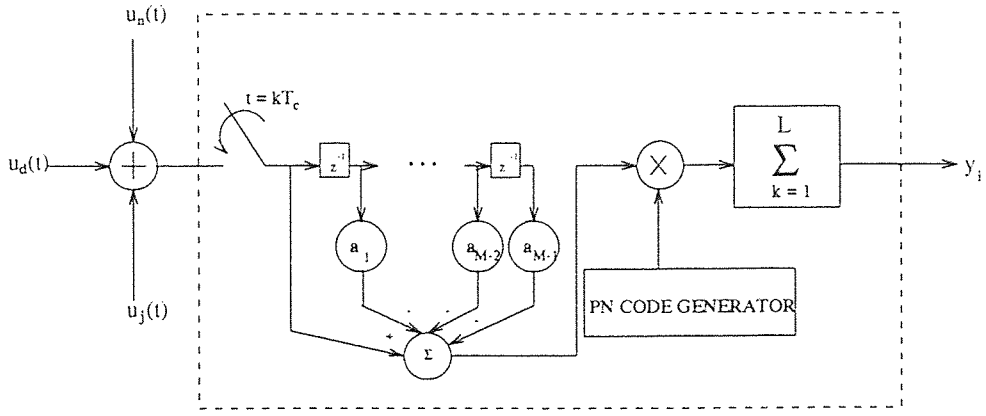

Figure 2.3 The adaptive interference-suppressant filter.

$$= \frac{L^2}{L\rho_j(0) + L\sigma_n^2}$$
$$= \frac{L}{J + \sigma_n^2}. \tag{2.4}$$

Given that the power of the modulated data signal $\sigma_d^2 = 1$, the SNIR improvement factor η of the processed signal is given as:

$$\eta = \frac{\text{SNIR}_f}{\text{SNIR}_{in}} = L. \tag{2.5}$$

2.2.2 The Adaptive Interference-Suppressant Filter

The adaptive interference-suppressant filter predicts the interference based upon past samples of the received signal and subtracts the interference estimate from the signal, a sample at a time. Linear prediction algorithms implemented by transversal filters may be used to estimate the interference signal [11]. An adaptive spread spectrum receiver consisting of a transversal filter followed by the spread spectrum demodulator is depicted in Figure 2.3.

Once the statistical properties of the interference are known or estimated, the weights can be adapted such that the sum of the product of each past sample with its respective tap-weight vector element yields an interference estimate. Subtracting this estimate from the current sample of an incoming signal on the first tap-weight

element of unity value removes the interference sample to a certain extent, thereby delivering a relatively interference-free signal.

The output of the M-tap filter y_k at time k is given as follows:

$$\begin{aligned} y_k &= u_k - \sum_{n=1}^{M-1} a_n u_{k-n} \\ &= u_k - \hat{u}_{j,k} \end{aligned} \tag{2.6}$$

where $\hat{u}_j$ is the interference estimate.

Let a_n and u_{k-n} be represented by $\mathbf{A}$ and $\mathbf{U}'_{\mathrm{k}}$, respectively, where $\mathbf{A} = [a_1 \ \cdots \ a_{M-1}]^H$ and $\mathbf{U}'_k = \left[u_{k-1} \ \cdots \ u_{k-(M-1)}\right]^T$. Therefore,

$$\begin{aligned} y_k &= u_k - \mathbf{A}^H \mathbf{U}_k \\ &= \mathbf{W}^H \mathbf{U}_k \end{aligned} \tag{2.7}$$

where $\mathbf{W} = [1 \ -\mathbf{A}^H]^H$ and $\mathbf{U}_k = [u_k \ \mathbf{U}_k'^T]^T$. Then, the output of the filter is fed to the demodulator.

The SNIR at the output of a receiver consisting of an interference-suppressant filter and a PN demodulator is defined below [15]:

$$\begin{aligned} \mathrm{SNIR}_{out} = \frac{\mathrm{E}^2[y_k]}{\mathrm{E}[|y_k - \mathrm{E}[y_k]|^2]} &= \frac{\mathrm{E}^2\left[\sum_{k=0}^{L} c_k \sum_{n=0}^{M-1} w_n u_{k-n}\right]}{\mathrm{E}\left[\left|\sum_{k=0}^{L} c_k \sum_{n=0}^{M-1} w_n u_{k-n} - \mathrm{E}\left[\sum_{k=0}^{L} c_k \sum_{n=0}^{M-1} w_n u_{k-n}\right]\right|^2\right]} \\ &= \frac{L^2}{L\sum_{m=1}^{M-1} w_m^2 + L\sum_{m=0}^{M-1}\sum_{l=0}^{M-1} w_m w_l \rho_j(m-l) + L\sigma_n^2 \sum_{m=0}^{M-1} w_m^2} \\ &= \frac{L}{\mathbf{W}^H\mathbf{W} - 1 + \mathbf{W}^H\mathcal{R}_I\mathbf{W} + \sigma_n^2\mathbf{W}^H\mathbf{W}} \\ &= \frac{L}{\mathbf{W}^H\mathcal{R}_I\mathbf{W} + (\sigma_n^2+1)\mathbf{W}^H\mathbf{W} - 1} \end{aligned} \tag{2.8}$$

where L is the size of the PN demodulator or the processing gain, ρ_j is the autocorrelation sequence of the interference, σ_n^2 is the variance or power of the thermal noise, and $\mathcal{R}_I$ is the autocorrelation matrix of the interference, given by the Toeplitz of ρ_j.

Combining Equations 2.4 and 2.8, the SNIR improvement factor $\eta^{'}$ of the adaptive filter receiver over the fixed matched filter is given by:

$$\eta^{'} = \frac{\mathrm{SNIR}_{out}}{\mathrm{SNIR}_{f}} = \frac{L}{\mathbf{W}^{H}\mathcal{R}_{I}\mathbf{W} + (\sigma_{n}^{2}+1)\mathbf{W}^{H}\mathbf{W} - 1} \cdot \frac{J+\sigma_{n}^{2}}{L} = \frac{J+\sigma_{n}^{2}}{\mathbf{W}^{H}\mathcal{R}_{I}\mathbf{W} + (\sigma_{n}^{2}+1)\mathbf{W}^{H}\mathbf{W} - 1} \tag{2.9}$$

where SNIR_{out} is the SNIR at the output of demodulator in an adaptive filter receiver, and SNIR_{f} is the SNIR at the output of a fixed matched filter. Therefore, the SNIR improvement factor of the adaptive filter receiver over the input to the receiver is equal to $L\eta^{'}$.

Another standard figure of merit in digital communications is the probability of error. At the output of the receiver, a decision has to be made regarding the transmitted signal bit based upon the processed data, e.g., in the case of a bi-polar signal, if a bit of value $+1$ was sent, the decision making involves choosing between -1 and $+1$. The probability of error yields the percentage of incorrect decisions made based upon the number of bits received. Assume the received bit has Gaussian statistics with mean squared and variance forming the numerator and the denominator of the SNIR at the output of the demodulator, respectively, as defined in Equation 2.8. Then, the probability of error P_e may be defined in terms of the $\mathcal{Q}$ function as follows [15]:

$$P_e = \mathcal{Q}\left(\sqrt{\mathrm{SNIR}_{out}}\right). \tag{2.10}$$

where $\mathcal{Q}(x) \triangleq 0.5\ \mathrm{erfc}\left(x/\sqrt{2}\right)$.

A standard figure of merit used to test the perturbation in the adaptive tap weights due to measurement noise is comparing the MS at the output of the filter to the minimum MS, defined by the MS at the input as follows:

$$\mathrm{E}[|y_k|^2]_{min} = \mathrm{E}[|u_k|^2] - \mathbf{W}_{o}^{H}\mathcal{R}\mathbf{W}_{o}.$$

Rearranging the equation given above yields the MS at the input of the filter u_k in terms of the desired minimum MS at the output of the filter:

$$\mathrm{E}\left[|u_k|^2\right] \;=\; \mathrm{E}\left[|y_k|^2\right]_{min} + \mathbf{W}_o^H \mathcal{R} \mathbf{W}_o.$$

Therefore, the interference term is given by the second item on the RHS of the equation. Placing this definition of $\mathrm{E}[|u_k|^2]$ in the derivation of $\mathrm{E}[|y_k|^2]$ yields:

$$\mathrm{E}\left[|y_k|^2\right] \;=\; \mathrm{E}\left[|y_k|^2\right]_{min} + (\mathbf{W}_o - \mathbf{W})^H \mathcal{R} (\mathbf{W}_o - \mathbf{W}) \tag{2.11}$$

where the second term on the RHS of the equation represents the MS excess noise. In keeping with the format adopted for the convergence in the mean, the last equation may be rewritten as:

$$\mathcal{J}(k) \;=\; \mathcal{J}_{min} + \mathcal{J}_{ex}(k) \tag{2.12}$$

where $\mathcal{J}_{ex}(k)$ is the *excess* MS beyond the minimum MS $\mathcal{J}_{min}$ which constitutes the MS of the output of the filter.

Another figure of merit is the normalized variance of a weight vector. The expression for the normalized variance is based on the premise $\hat{\mathcal{R}}\hat{\mathbf{W}} = \mathbf{u}_s$ where $\mathbf{u}_s$ varies from filter to filter. Let $\hat{\mathcal{R}} = \mathcal{R} + \Delta\mathcal{R}$, where $\Delta\mathcal{R}$ is the perturbation in the autocorrelation matrix. Likewise, let $\hat{\mathbf{W}} = \mathbf{W} + \Delta\mathbf{W}$, where $\mathbf{W}$ is the optimal weight vector and $\Delta\mathbf{W}$ is the perturbation in the weight vector. The normalized variance of a weight vector is given by,

$$\mathrm{E}\left[\frac{\|\Delta\mathbf{W}\|^2}{\|\mathbf{W}\|^2}\right] = \frac{\mathrm{E}\left[\|\hat{\mathbf{W}} - \mathbf{W}\|^2\right]}{\mathbf{W}^H\mathbf{W}} \tag{2.13}$$

where the term in the numerator is the square of the norm of the weight vector perturbation and the term in the denominator is the square of the norm of the optimal weight vector, alternatively the Wiener-Hopf or the Eigencanceler, as appropriate.

In summary, the corrupted signal passes through an interference-suppressant filter and then through a PN demodulator matched to the one in the transmitter.

The filter exploits the coherence or correlation properties of the narrow-band interference in order to predict it and subtract it from the received signal [11]. The PN demodulator averages spread the interference over the entire spread spectrum and then reduce the interference contribution by averaging the noise-like signal.

Now that the parameters of both the signal model and the receiver have been covered extensively, the next step is to examine the optimal solution for the excision of narrow-band interference in a white Gaussian environment.

2.3 The Wiener-Hopf

The prediction error e_k is the difference between the actual interference sample $u_{j,k}$ and the interference estimate $\hat{u}_{j,k}$ at time k; then,

$$e_k = u_{j,k} - \hat{u}_{j,k}.$$

The Wiener-Hopf filter minimizes the mean-square prediction error (MSE). The output y_k of the M-tap filter at time k is given by Equation 2.6:

$$\begin{aligned} y_k &= u_k - \sum_{n=1}^{M-1} a_n u_{k,n} \\ &= u_k - \hat{u}_{j,k}. \end{aligned}$$

Due to the independence between the data signal, the interference, and the thermal noise, minimizing $\mathrm{E}\left[|e_k|^2\right]$ is equivalent to minimizng the mean-square (MS) at the output of the filter. Therefore, the output y_k may be re-written in terms of the prediction error e_k:

$$\begin{aligned} e_k &= u_k - \mathbf{A}^H \mathbf{U}_k' \\ &= \mathbf{W}^H \mathbf{U}_k. \end{aligned}$$

Therefore the MSE term may be expressed as:

$$\begin{aligned} \mathrm{E}\left[|e_k|^2\right] &= \mathbf{W}^H \mathrm{E}\left[\mathbf{U}_k \mathbf{U}_k^T\right] \mathbf{W} \\ &= \mathbf{W}^H \mathcal{R} \mathbf{W}. \end{aligned}$$

We seek to minimize $\mathrm{E}\left[|e_k|^2\right]$ with respect to $\mathbf{W}^H$, with the constraint that the reference tap-weight $\mathbf{W}(1)$ be equal to one because the current signal sample u_k on the first tap-weight element is the *reference* signal sample. Accordingly, using the Lagrange multiplier method, we solve for the following expression:

$$\min_{\mathbf{W}^H} \mathbf{W}^H \mathcal{R} \mathbf{W} \text{ subject to } \mathbf{W}^H \mathbf{u}_o = 1$$

where $\mathbf{u}_o = [1\ 0\ \ldots\ 0]$.

The gradient $\mathcal{J}$ to be minimized is set up as follows:

$$\mathcal{J} = \mathbf{W}^H \mathcal{R} \mathbf{W} + \lambda_1 \left(1 - \mathbf{W}^H \mathbf{u}_o\right)$$

where λ_1 is the Lagrange multiplier. Minimizing $\mathcal{J}$ with respect to $\mathbf{W}^H$:

$$\nabla \mathcal{J} = \mathcal{R}\mathbf{W} - \lambda_1 \mathbf{u}_o = 0.$$

Therefore, the weight vector is defined as follows:

$$\mathbf{W} = \lambda_1 \mathcal{R}^{-1} \mathbf{u}_o.$$

To solve for the Lagrange multiplier, the sole constraint is taken into account:

$$\mathbf{W}^H \mathbf{u}_o = \lambda_1^* \mathbf{u}_o^T \mathcal{R}^{-1} \mathbf{u}_o = 1.$$

Therefore,

$$\lambda_1 = \lambda_1^* = \frac{1}{\mathbf{u}_o^T \mathcal{R}^{-1} \mathbf{u}_o}.$$

Thus, the optimal weight vector $\mathbf{W}_o$ that minimizes the MS at the output of the interference-suppressant filter is given by:

$$\mathbf{W}_o = \frac{\mathcal{R}^{-1} \mathbf{u}_o}{\mathbf{u}_o^T \mathcal{R}^{-1} \mathbf{u}_o}. \tag{2.14}$$

Equation 2.14 is the optimal tap-weight vector for suppressing a band-limited interference when the autocorrelation matrix of the interference is known.

2.4 The Widrow-Hoff LMS

The LMS and RLS were introduced as Wiener-based recursive algorithms. Their derivation and their convergence rate to the Wiener-Hopf solution will be covered in this and the following section.

The LMS algorithm updates the adaptive tap-weights $\mathbf{A}_k$ of the weight vector $\mathbf{W}_k = \begin{bmatrix} 1 & -\mathbf{A}_k^H \end{bmatrix}^H$ at time k as follows:

$$\mathbf{A}_k = \mathbf{A}_{k-1} + \mu y_k \mathbf{U}_k' \tag{2.15}$$

where μ is a fixed step-size parameter and $y_k = u_k - \mathbf{A}_{k-1}^H \mathbf{U}_k'$ is the output of the un-updated filter. $\mathbf{A}_{k-1}$ is the $(k-1)$-th iteration of the adaptive tap-weights, and $\mathbf{U}_k'$ is the vector of the $(M-1)$ past samples of the received signal on the filter tap-weights.

The LMS minimizes the MS at the output of the filter, at each successive iteration, to converge to the minimum MS attained by the Wiener-Hopf filter. In order to converge to this point, the LMS must converge in the MS at the output of the filter, and it must converge in the mean of the weight vector $\mathbf{A}_k$ to the Wiener-Hopf filter $\mathbf{A}_o$ [10]. To converge in the mean of $\mathbf{A}_k$ to $\mathbf{A}_o$, the step-size μ is limited to the following:

$$0 < \mu < \frac{2}{\lambda_{max}'}$$

where λ_{max}' is the maximum eigenvalue of the autocorrelation matrix $\mathcal{R}' \triangleq \mathrm{E}\left[\mathbf{U}_k' \mathbf{U}_k'^T\right]$.

The convergence rate of $\mathbf{A}_k$ to $\mathbf{A}_o$ is determined by the ratio $\mathrm{E}\left[\frac{\|\varepsilon_{k+1}\|^2}{\|\varepsilon_k\|^2}\right]$, where $\varepsilon_k = \mathbf{A}_k - \mathbf{A}_o$. Accordingly, we derive the convergence rate from (9.74) of [10]:

$$\mathcal{K}_{k+1} = \mathcal{K}_k - \mu\left[\mathcal{R}'\mathcal{K}_k + \mathcal{K}_k\mathcal{R}'\right] + \mu^2\mathcal{R}'\mathrm{tr}\left[\mathcal{R}'\mathcal{K}_k\right] + \mu^2\mathcal{R}'\mathcal{K}_k\mathcal{R}' + \mu^2\mathcal{J}_{min}\mathcal{R}' \tag{2.16}$$

where $\mathcal{K}_k \triangleq \mathrm{E}[\varepsilon_k\varepsilon_k^H]$ is the weight vector error covariance matrix, and $\mathcal{J}_{min}$ is the minimum MSE at the output of the filter.

Taking advantage of the definition $\mathrm{E}\left[\|\varepsilon_k\|^2\right] \triangleq \mathrm{tr}\left[\mathcal{K}_k\right]$, and $\mathcal{R}' \simeq \sigma_u^2\mathbf{I}$, where $\sigma_u^2 \triangleq \mathrm{E}\left[u_k^2\right]$, $\mathrm{tr}\left[\mathcal{R}'\right] = (M-1)\sigma_u^2$, and $\mathrm{tr}\left[\mathcal{K}_k\mathcal{R}'\right] = \sigma_u^2\,\mathrm{tr}\left[\mathcal{K}_k\right]$, the trace of both sides of Equation 2.16 yields

$$\mathrm{E}\left[\|\varepsilon_{k+1}\|^2\right] \simeq \left[1 - 2\mu\sigma_u^2 + \mu^2 M\sigma_u^4\right]\mathrm{E}\left[\|\varepsilon_k\|^2\right] \tag{2.17}$$

where $\mathcal{J}_{min}$ is ignored. The minimization of the term $[1 - 2\mu\sigma_u^2 + \mu^2 M\sigma_u^4]$ yields the optimal rate of covergence for the LMS. Accordingly, $\mu_{opt} = \dfrac{1}{M\sigma_u^2}$. Therefore, Equation 2.17 may be re-written as:

$$\mathrm{E}\left[\|\varepsilon_{k+1}\|^2\right] \simeq \frac{M-1}{M}\mathrm{E}\left[\|\varepsilon_k\|^2\right] \tag{2.18}$$

where M is the length of the interference-suppressant filter.

Given that the initial $\mathbf{A}_{k=0} = \mathbf{0}$, $\varepsilon_0 = -\mathbf{A}_o$. Therefore, the convergence rate of $\mathbf{A}_k$ to $\mathbf{A}_o$ at time k may be expressed as:

$$\mathrm{E}\left[\|\varepsilon_k\|^2\right] \simeq \left(\frac{M-1}{M}\right)^k \mathrm{E}\left[\|\mathbf{A}_o\|^2\right]. \tag{2.19}$$

Both the ratio $\mathrm{E}\left[\dfrac{\|\varepsilon_{k+1}\|^2}{\|\varepsilon_k\|^2}\right]$ and $\mathrm{E}\left[\|\varepsilon_k\|^2\right]$ demonstrate a dependence on the length M of the adaptive filter. The larger M is, the longer it takes the term $\mathrm{E}\left[\|\varepsilon_k\|^2\right]$ to converge.

Equations 2.11 and 2.12 present the convergence of an algorithm in the MS at the output of the filter. Haykin gives the MS at the output of the filter in (9.81) of [10], re-written here:

$$\mathcal{J}(k) = \mathcal{J}_{min} + \mathrm{tr}\left[\mathcal{R}'\mathcal{K}_k\right]. \tag{2.20}$$

From Equations 2.17 and 2.19, Equation 2.20 may be re-written as:

$$\begin{aligned}\mathcal{J}(k) &= \mathcal{J}_{min} + \sigma_u^2\mathrm{E}\left[\|\varepsilon_k\|^2\right] \\ &= \mathcal{J}_{min} + \sigma_u^2\left(\frac{M-1}{M}\right)^k \mathrm{E}\left[\|\mathbf{A}_o\|^2\right].\end{aligned} \tag{2.21}$$

Equation 2.21 represents the convergence of the MS $\mathcal{J}(k)$ at the output of the adaptive filter at every iteration k. Like the convergence of the weight vector perturbation ε_k, $\mathcal{J}(k)$ also demonstrates a dependence on M.

2.5 The RLS

The RLS updates the adaptive tap-weights at time k as follows:

Initialize the RLS:

$$\begin{aligned} \mathbf{\Phi}_0 &= \delta^{-1}\mathbf{I} \\ \mathbf{A}_{k=0} &= 0 \end{aligned}$$

where $\mathbf{\Phi}_k$ is the inverse of the *time-averaged* autocorrelation matrix $\hat{\mathcal{R}}_k'$ of the $(M-1)$ past samples of the received signal on the adaptive tap-weights at time k, δ is a small positive constant, and $\mathbf{I}$ is the identity matrix.

At every k-th iteration, the RLS updates the following parameters:

The gain vector:

$$\mathcal{G}_k = \frac{\mathbf{\Phi}_{k-1}\mathbf{U}_k'}{\gamma + \mathbf{U}_k'^T\mathbf{\Phi}_{k-1}\mathbf{U}_k'}$$

where $\mathcal{G}_k$ is the variable step-size, a.k.a. the *gain vector*, and γ is the forgetting factor.

The adaptive tap-weight vector:

$$\mathbf{A}_k = \mathbf{A}_{k-1} + \mathcal{G}_k y_k \tag{2.22}$$

where $y_k = u_k - \mathbf{A}_{k-1}^H\mathbf{U}_k'$ is the output of the un-updated filter.

The inverse of the correlation matrix:

$$\mathbf{\Phi}_k = \frac{1}{\gamma}\left[\mathbf{I} - \mathcal{G}_k\mathbf{U}_k'\right]\mathbf{\Phi}_{k-1}.$$

Like the LMS, the RLS is to be evaluated at the convergence of the weight vector in the mean and in the MS at the output of the filter. For the RLS, the convergence rate of $\mathbf{A}_k$ to the Wiener-Hopf filter $\mathbf{A}_o$ is developed using the ratio $\mathrm{E}\left[\frac{\|\varepsilon_{k+1}\|^2}{\|\varepsilon_k\|^2}\right]$. We use the expression (13.41) of [10] to establish the relation between $\mathcal{K}_k$ and $\mathbf{\Phi}_k$:

$$\mathcal{K}_k \triangleq \mathrm{E}\left[\varepsilon_k\varepsilon_k^H\right] = \lambda_{min}'\mathbf{\Phi}_k.$$

The equation given above may be re-written in terms of the *ensemble-averaged* autocorrelation matrix $\mathcal{R}'$ of the $(M-1)$ past signal samples, using the approximation $\mathcal{R}' \simeq \frac{1}{k}\mathbf{\Phi}_k^{-1}$ in (13.42) of [10]. Hence,

$$\mathcal{K}_k = \frac{\lambda'_{min}}{k}\mathcal{R}'^{-1} \tag{2.23}$$

where λ'_{min} is the minimum eigenvalue of $\mathcal{R}$. Accordingly,

$$\mathrm{E}\left[\|\varepsilon_k\|^2\right] \simeq \frac{\lambda'_{min}}{k}\mathrm{tr}\left[\mathcal{R}'^{-1}\right]. \tag{2.24}$$

Therefore, the convergence ratio is given by

$$\mathrm{E}\left[\frac{\|\varepsilon_{k+1}\|^2}{\|\varepsilon_k\|^2}\right] = \frac{k}{k+1}. \tag{2.25}$$

Employing the same initial conditions used in the LMS, the convergence rate of $\mathbf{A}_k$ to $\mathbf{A}_o$ at time k is given by:

$$\mathrm{E}\left[\|\varepsilon_k\|^2\right] \simeq \frac{1}{k+1}\mathrm{E}\left[\|\mathbf{A}_o\|^2\right]. \tag{2.26}$$

Note that the convergence rate for the weight vector in the RLS algorithm depends on the k-th iteration, thereby giving the RLS a significant initial advantage over the LMS in Equation 2.19 in convergence to the optimal solution. Equally significantly, the convergence rate is *independent* of the length of the adaptive filter M.

The MS at the output of the filter is

$$\mathcal{J}(k) = \mathcal{J}_{min} + \mathrm{tr}\left[\mathcal{R}'\mathcal{K}_k\right]. \tag{2.27}$$

Given the definitions derived in Section 2.4, Equation 2.27 may be written as:

$$\mathcal{J}(k) \simeq \mathcal{J}_{min} + \sigma_u^2\frac{1}{k+1}\mathrm{E}\left[\|\mathbf{A}_o\|^2\right]. \tag{2.28}$$

Like the convergence of the weight vector perturbation ε_k, $\mathcal{J}(k)$ also demonstrates a dependence on the k-th iteration.

CHAPTER 3

THE EIGENCANCELER

The previous chapters introduced the implementation of the Wiener-Hopf filter and the LMS and RLS algorithms in a spread spectrum system. However, the Wiener-Hopf and the Wiener-Hopf based algorithms have demonstrated sensitivity to the measurement noise. Furthermore, the chief detraction of the LMS is its sensitivity to the eigenvalue-spread. The *Eigencanceler* offers a new approach in the excision of correlated information in a white Gaussian environment by using an eigenanalysis-based method, which will prove to be insensitive to measurement noise.

The received signal may be represented in terms of the eigenvalues and eigenvectors of its autocorrelation matrix. As both the modulated data signal and thermal noise are white, their eigenvalue terms are small and spread throughout the entire signal eigen-space, i.e., they span *all* eigenvectors of the signal space. This does not apply to narrow-band interference, since the interference is entirely concentrated in a few eigenvectors of the signal eigen-space, termed the interference subspace. The high-power narrow-band interference may be located by examining the large eigenvalues it generates in the autocorrelation matrix of the received signal. Moreover, the interference subspace is orthogonal to the noise subspace where the majority of the modulated data signal and thermal noise are concentrated. Therefore, a tap-weight vector residing in the noise subspace will effectively cancel the interference, leaving most of the modulated data signal and thermal noise untouched.

Given an environment, where only a finite set of samples of the received signal are given, with unknown correlation statistics, subsequent computations yield an estimate of the autocorrelation matrix of the received signal. In a stationary environment, as more data is collected and analyzed, the estimate of the autocorrelation matrix improves, thereby yielding a better interference-suppressant filter.

However, in a highly non-stationary environment the data size is significantly limited. Given that the time-averaged autocorrelation matrix is an estimate of the ensemble-averaged autocorrelation matrix, and given that the noise samples vary from set to set, the eigen-decomposition reveals that the noise eigenvalues constantly fluctuate and are uneven. This inconsistency masks the interference to a significant extent, thereby slowing down the convergence of the Wiener-Hopf to the Wiener-Hopf solution based on known signal statistics. The Wiener-Hopf is dependent upon matrix inversion for estimation of the interference. The matrix inversion causes small eigenvalues to be inverted as well, thereby increasing the impact of the noise on the interference estimate. As the Eigencanceler does not employ eigenvalues, it is unaffected by fluctuations in the noise eigenvalues; hence, a rapid convergence to the optimal solution. Even with a few data, it is possible to perform an eigenanalysis of the received signal so as to determine the interference subspace. Consequently, the Eigencanceler algorithm is able to achieve a high degree of interference cancellation within relatively far fewer samples than is needed for the Wiener-Hopf, the LMS and the RLS to yield the same system performance.

In conclusion, while the Wiener-Hopf is the optimal solution given the correlation statistics of the received signal, the Eigencanceler proves to be superior, though sub-optimal, in the lack thereof.

This chapter will be divided as follows: Section 3.1 covers the eigenanalysis of the received signal. Section 3.2 derives a filter which combines both the Wiener-Hopf and Eigencanceler methods. Section 3.3 derives the Eigencanceler. Simulation results comparing the Eigencanceler method with the Wiener-Hopf are presented in Chapter 5.

3.1 Eigenanalysis of the Signal Model

From Chapter 2, the ensemble-averaged autocorrelation matrices of the signal model with a single tone interference and with a single narrow-band Gaussian interference are given by Equations 2.2 and 2.3, respectively. The independence between the interferences and noise, i.e., the modulated data signal and thermal noise, allows for the separation of the autocorrelation matrices of interference and noise as follows:

$$\mathcal{R} = \mathcal{R}_I + \mathcal{R}_\nu$$

where $\mathcal{R}_I$ and $\mathcal{R}_\nu$ are the autocorrelation matrices of the interference and noise, respectively.

From [6], performing an eigenanalysis of the equation given above yields

$$\begin{aligned} \mathcal{R} &= \mathbf{Q}_I \Lambda_I \mathbf{Q}_I^H + \mathbf{Q}_\nu \Lambda_\nu \mathbf{Q}_\nu^H \\ &= \mathbf{Q}_I \Lambda_I \mathbf{Q}_I^H + \sigma_\nu^2 \mathbf{Q}_\nu \mathbf{Q}_\nu^H \end{aligned} \tag{3.1}$$

where $\mathbf{Q}_I$ and $\mathbf{Q}_\nu$ are matrices whose columns contain the interference and noise eigenvectors, respectively, and Λ_I and Λ_ν are the corresponding diagonal eigenvalue matrices. Since the noise is white, all of its eigenvalues are equal to σ_ν^2, which is the power or variance of the noise; hence, the second term on the RHS of Equation 3.1.

In practical situations, the correlation statistics of the received signal are unknown and have to be estimated. Hence, the autocorrelation matrix is time-averaged and is given by:

$$\begin{aligned} \hat{\mathcal{R}} &= \hat{\mathbf{Q}}_I \hat{\Lambda}_I \hat{\mathbf{Q}}_I^H + \hat{\mathbf{Q}}_\nu \hat{\Lambda}_\nu \hat{\mathbf{Q}}_\nu^H \\ &= \sum_{n=1}^{p} \hat{\lambda}_n \hat{\mathbf{q}}_n \hat{\mathbf{q}}_n^H + \sum_{n=p+1}^{M} \hat{\lambda}_n \hat{\mathbf{q}}_n \hat{\mathbf{q}}_n^H \end{aligned} \tag{3.2}$$

where $\hat{\lambda}$'s are the eigenvalues, $\hat{\mathbf{q}}$'s are the eigenvectors, p is the size of the interference subspace or number of degrees of freedom occupied by the interference, and M is the total number of degrees of freedom occupied by the received signal. Note that

$\hat{\Lambda}_\nu$ contains small and *uneven* eigenvalues $\hat{\lambda}_n, n = p+1 \ldots M$, in contrast to Λ_ν in Equation 3.1 which contains small but *equal* eigenvalues of value σ_ν^2.

As the Wiener-Hopf and the algorithms based on the Wiener-Hopf rely upon the inversion of the autocorrelation matrix, the eigenvalues too are inverted, with the result that the large eigenvalues have little impact on the Wiener-Hopf whereas the small eigenvalues have a significant impact as shown below. Due to the orthonormality property between $\mathbf{Q}_I$ and $\mathbf{Q}_\nu$, the eigen-decomposition of the inverse of the ensemble-averaged autocorrelation matrix yields:

$$\mathcal{R}^{-1} = \mathbf{Q}_I \Lambda_I^{-1} \mathbf{Q}_I^H + \frac{1}{\sigma_\nu^2} \mathbf{Q}_\nu \mathbf{Q}_\nu^H. \tag{3.3}$$

The eigen-decomposition of the inverse of the time-averaged autocorrelation matrix yields:

$$\begin{aligned} \hat{\mathcal{R}}^{-1} &= \hat{\mathbf{Q}}_I \hat{\Lambda}_I^{-1} \hat{\mathbf{Q}}_I^H + \hat{\mathbf{Q}}_\nu \hat{\Lambda}_\nu^{-1} \hat{\mathbf{Q}}_\nu^H \\ &= \sum_{n=1}^{p} \frac{1}{\hat{\lambda}_n} \hat{\mathbf{q}}_n \hat{\mathbf{q}}_n^H + \sum_{n=p+1}^{M} \frac{1}{\hat{\lambda}_n} \hat{\mathbf{q}}_n \hat{\mathbf{q}}_n^H. \end{aligned} \tag{3.4}$$

The second term on the RHS illustrates the impact of the inverse of the small eigenvalues on the development of the Wiener-Hopf.

Let $\mathbf{Q}$ be the eigenvector matrix that comprises the signal space such that $\mathbf{Q} = [\mathbf{Q}_I : \mathbf{Q}_\nu]$. From [10] and the unitary property of $\mathbf{Q}$, we find that $\mathbf{Q}\mathbf{Q}^H = I$. Therefore, due to the orthonormality between $\mathbf{Q}_I$ and $\mathbf{Q}_\nu$, we can deduce that

$$\hat{\mathbf{Q}}_I \hat{\mathbf{Q}}_I^H + \hat{\mathbf{Q}}_\nu \hat{\mathbf{Q}}_\nu^H = I. \tag{3.5}$$

Equation 3.5 represents the interference and the noise in terms of the respective subspaces they occupy, a trait of the received signal that shall prove useful in the derivation of the Eigencanceler in the Section 3.3.

In light of the focus of this work, the weight vectors involved here are best dealt with from an eigenanalysis point of view. Hence, the Wiener-Hopf, given by

Equation 2.14, may be re-defined as follows:

$$\mathbf{W}_o = \frac{[\mathbf{Q}_I \Lambda_I^{-1} \mathbf{Q}_I^H + \mathbf{Q}_\nu \Lambda_\nu^{-1} \mathbf{Q}_\nu^H]\mathbf{u}_o}{\mathbf{u}_o^T[\mathbf{Q}_I \Lambda_I^{-1} \mathbf{Q}_I^H + \mathbf{Q}_\nu \Lambda_\nu^{-1} \mathbf{Q}_\nu^H]\mathbf{u}_o}. \tag{3.6}$$

In a highly negative SIR environment, $\lambda_n|_{n=1\ldots p} \gg \lambda_n|_{n=p+1\ldots M} = \sigma_\nu^2$. Under such conditions, Equation 3.6 may be approximated by,

$$\mathbf{W}_o \simeq \frac{\mathbf{Q}_\nu \Lambda_\nu^{-1} \mathbf{Q}_\nu^H \mathbf{u}_o}{\mathbf{u}_o^T \mathbf{Q}_\nu \Lambda_\nu^{-1} \mathbf{Q}_\nu^H \mathbf{u}_o} = \frac{\mathbf{Q}_\nu \mathbf{Q}_\nu^H \mathbf{u}_o}{\mathbf{u}_o^T \mathbf{Q}_\nu \mathbf{Q}_\nu^H \mathbf{u}_o}. \tag{3.7}$$

The Wiener-Hopf filter minimizes the MS at the output of the filter, derived in the previous section. The following term is the minimum MS attained by the Wiener-Hopf:

$$\begin{aligned} \mathcal{J}_{min} = \mathbf{W}_o^H \mathcal{R} \mathbf{W}_o = \frac{\mathbf{u}_o^T \mathcal{R}^{-1} \mathbf{u}_o}{(\mathbf{u}_o^T \mathcal{R}^{-1} \mathbf{u}_o)^2} &= \frac{1}{\mathbf{u}_o^T \mathcal{R}^{-1} \mathbf{u}_o} \\ &= \frac{1}{\mathbf{u}_o^T \left[\mathbf{Q}_I \Lambda_I^{-1} \mathbf{Q}_I^H + \sigma_\nu^{-2} \mathbf{Q}_\nu \mathbf{Q}_\nu^H\right] \mathbf{u}_o}. \end{aligned} \tag{3.8}$$

Under highly negative SIR conditions, Equation 3.8 may be approximated by,

$$\mathcal{J}_{min} \simeq \frac{\sigma_\nu^2}{\mathbf{u}_o^T \mathbf{Q}_\nu \mathbf{Q}_\nu^H \mathbf{u}_o}. \tag{3.9}$$

The Wiener-Hopf based on the time-averaged autocorrelation matrix is given by,

$$\hat{\mathbf{W}}_o = \frac{[\hat{\mathbf{Q}}_I \hat{\Lambda}_I^{-1} \hat{\mathbf{Q}}_I^H + \hat{\mathbf{Q}}_\nu \hat{\Lambda}_\nu^{-1} \hat{\mathbf{Q}}_\nu^H]\mathbf{u}_o}{\mathbf{u}_o^T[\hat{\mathbf{Q}}_I \hat{\Lambda}_I^{-1} \hat{\mathbf{Q}}_I^H + \hat{\mathbf{Q}}_\nu \hat{\Lambda}_\nu^{-1} \hat{\mathbf{Q}}_\nu^H]\mathbf{u}_o}. \tag{3.10}$$

Again, in a highly negative SIR environment, Equation 3.10 may be approximated by,

$$\hat{\mathbf{W}}_o \simeq \frac{\hat{\mathbf{Q}}_\nu \hat{\Lambda}_\nu^{-1} \hat{\mathbf{Q}}_\nu^H \mathbf{u}_o}{\mathbf{u}_o^T \hat{\mathbf{Q}}_\nu \hat{\Lambda}_\nu^{-1} \hat{\mathbf{Q}}_\nu^H \mathbf{u}_o} \tag{3.11}$$

where $\hat{\Lambda}_\nu$ contains small but *uneven* noise eigenvalues pertaining to the time-averaged autocorrelation matrix of the received signal.

The normalized variance of the Wiener-Hopf, defined by Equation 2.13, is given in [9]:

$$\mathrm{E}\left[\frac{\|\Delta \mathbf{W}_o\|^2}{\|\mathbf{W}_o\|^2}\right] = \frac{1}{M}. \tag{3.12}$$

where $\Delta \mathbf{W}_o = \hat{\mathbf{W}}_o - \mathbf{W}_o$ is the weight vector perturbation. $\Delta \mathbf{W}_o$ is thus dependent on the rank M, of $\mathcal{R}$ *and*, thereby, also the length of the interference-suppressant filter. The longer the filter, the better the estimation of the interference; hence, an increase in robustness to measurement noise.

3.2 The Constrained Minimum Variance Filter

The Wiener-Hopf minimizes the MS at the output of the filter with the constraint that the first tap-weight element be of unity value. The Eigencanceler is designed under different conditions, and it is subject to an additional constraint, namely, that it is orthogonal to the interference subspace.

In order to understand the fundamental differences between the two methods, it is necessary to develop an intermediate step, that of constructing a filter based on the Wiener-Hopf concept of minimizing the MS, i.e., $\mathbf{W}^H \mathcal{R} \mathbf{W}$ and on the Eigencanceler concept of being orthogonal to the interference subspace. As the environment is random white Gaussian, the means of both the input and the output are equal to zero. In addition, the adaptive filter is linear and transversal. Hence, the intermediate method may be characterized as a linearly *constrained minimum variance* (CMV) filter [10].

The objective of the CMV filter is to minimize the interference and the noise by applying several constraints via the Lagrange multiplier method as follows:

$$\min_{\mathbf{W}^H} \mathbf{W}^H \mathcal{R} \mathbf{W} \text{ subject to: } (1)\mathbf{W}^H \mathbf{q}_I = 0 \text{ and } (2)\mathbf{W}^H \mathbf{u}_o = 1$$

where $\mathbf{q}_I$ is a single interference eigenvector for an interference occupying a 1-D eigen-space and $\mathbf{u}_o = [1\ 0 \ldots 0]^T$.

The gradient $\mathcal{J}$ to be minimized is set up as follows:

$$\mathcal{J} = \mathbf{W}^H \mathcal{R} \mathbf{W} + \lambda_1 (1 - \mathbf{W}^H \mathbf{u}_o) + \lambda_2 (-\mathbf{W}^H \mathbf{q}_I)$$

where $[\lambda_1, \lambda_2]$ are the two Lagrange multipliers. Minimizing $\mathcal{J}$ with respect to $\mathbf{W}$:

$$\nabla \mathcal{J} = \mathcal{R}\mathbf{W} - \lambda_1 \mathbf{u}_o - \lambda_2 \mathbf{q}_I = 0.$$

Therefore, the weight vector is defined as follows:

$$\mathbf{W} = \lambda_1 \mathcal{R}^{-1}\mathbf{u}_o + \lambda_2 \mathcal{R}^{-1}\mathbf{q}_I.$$

To solve for the two Lagrange multipliers, the first constraint is taken into account:

$$\mathbf{W}^H \mathbf{q}_I = \lambda_1^* \mathbf{u}_o^T \mathcal{R}^{-1}\mathbf{q}_I + \lambda_2^* \mathbf{q}_I^H \mathcal{R}^{-1}\mathbf{q}_I = 0.$$

Therefore,

$$\lambda_2^* = -\lambda_1^* \frac{\mathbf{u}_o \mathcal{R}^{-1}\mathbf{q}_I}{\mathbf{q}_I^H \mathcal{R}^{-1}\mathbf{q}_I} = -\lambda_1^* \frac{\frac{1}{\lambda_I}\mathbf{u}_o^T \mathbf{q}_I}{\frac{1}{\lambda_I}\mathbf{q}_I^H \mathbf{q}_I} = -\lambda_1^* \mathbf{u}_o^T \mathbf{q}_I$$

because, $\mathcal{R}^{-1}\mathbf{q}_I = \frac{1}{\lambda_I}\mathbf{q}_I$, where λ_I is the interference eigenvalue, and $\mathbf{q}_I^H \mathbf{q}_I = 1$. Therefore, $\lambda_2 = -\lambda_1 \mathbf{q}_I^H \mathbf{u}_o$.

Solving for the second constraint:

$$\mathbf{W}^H \mathbf{u}_o = \lambda_1^* \mathbf{u}_o^T \mathcal{R}^{-1}\mathbf{u}_o + \lambda_2^* \mathbf{q}_I^H \mathcal{R}^{-1}\mathbf{u}_o = 1.$$

Solving for $[\lambda_1, \lambda_2]$:

$$\begin{aligned}
\lambda_1^* [\mathbf{u}_o^T \mathcal{R}^{-1}\mathbf{u}_o + \mathbf{u}_o^T \mathbf{q}_I \mathbf{q}_I^H \mathcal{R}^{-1}\mathbf{u}_o] &= 1 \\
\lambda_1^* \mathbf{u}_o^T [I - \mathbf{q}_I \mathbf{q}_I^H] \mathcal{R}^{-1}\mathbf{u}_o &= 1 \\
\lambda_1 \mathbf{u}_o^T \mathcal{R}^{-1} [I - \mathbf{q}_I \mathbf{q}_I^H] \mathbf{u}_o &= 1.
\end{aligned}$$

Therefore,

$$\begin{aligned}
\lambda_1 &= \frac{1}{\mathbf{u}_o^T \mathcal{R}^{-1} [I - \mathbf{q}_I \mathbf{q}_I^H] \mathbf{u}_o} \\
\lambda_2 &= \frac{-\mathbf{q}_I^H \mathbf{u}_o}{\mathbf{u}_o^T \mathcal{R}^{-1} [I - \mathbf{q}_I \mathbf{q}_I^H] \mathbf{u}_o}.
\end{aligned}$$

Lastly, the CMV filter is derived below:

$$\begin{aligned}
\mathbf{W}_{CM} &= \lambda_1 \mathcal{R}^{-1}\mathbf{u}_o + \lambda_2 \mathcal{R}^{-1}\mathbf{q}_I \\
&= \frac{\mathcal{R}^{-1}\mathbf{u}_o - \mathcal{R}^{-1}\mathbf{q}_I \mathbf{q}_I^H \mathbf{u}_o}{\mathbf{u}_o^T \mathcal{R}^{-1} [I - \mathbf{q}_I \mathbf{q}_I^H] \mathbf{u}_o} \\
&= \frac{\mathcal{R}^{-1} [I - \mathbf{q}_I \mathbf{q}_I^H] \mathbf{u}_o}{\mathbf{u}_o^T \mathcal{R}^{-1} [I - \mathbf{q}_I \mathbf{q}_I^H] \mathbf{u}_o}.
\end{aligned} \tag{3.13}$$

The weight vector defined above meets the two specified constraints:

$$\mathbf{W}_{CM}^H \mathbf{u}_o = \frac{\mathbf{u}_o^T[I - \mathbf{q}_I\mathbf{q}_I^H]\mathcal{R}^{-1}\mathbf{u}_o}{\mathbf{u}_o^T[I - \mathbf{q}_I\mathbf{q}_I^H]\mathcal{R}^{-1}\mathbf{u}_o} = 1$$

$$\begin{aligned}\mathbf{W}_{CM}^H \mathbf{q}_I &= \frac{\mathbf{u}_o^T[I - \mathbf{q}_I\mathbf{q}_I^H]\mathcal{R}^{-1}\mathbf{q}_I}{\mathbf{u}_o^T[I - \mathbf{q}_I\mathbf{q}_I^H]\mathcal{R}^{-1}\mathbf{u}_o} \\ &= \frac{1}{\lambda_I}\frac{\mathbf{u}_o^T[I - \mathbf{q}_I\mathbf{q}_I^H]\mathbf{q}_I}{\mathbf{u}_o^T[I - \mathbf{q}_I\mathbf{q}_I^H]\mathcal{R}^{-1}\mathbf{u}_o} \\ &= \frac{1}{\lambda_I}\frac{\mathbf{u}_o^T[\mathbf{q}_I - \mathbf{q}_I]}{\mathbf{u}_o^T[I - \mathbf{q}_I\mathbf{q}_I^H]\mathcal{R}^{-1}\mathbf{u}_o} = 0.\end{aligned}$$

For the general case where there are p number of interference eigenvalues and eigenvectors, the CMV filter may be redefined as follows for an ensemble-averaged autocorrelation matrix $\mathcal{R}$:

$$\begin{aligned}\mathbf{W}_{CM} &= \frac{\mathcal{R}^{-1}[I - \mathbf{Q}_I\mathbf{Q}_I^H]\mathbf{u}_o}{\mathbf{u}_o^T\mathcal{R}^{-1}[I - \mathbf{Q}_I\mathbf{Q}_I^H]\mathbf{u}_o} \\ &= \frac{\frac{1}{\sigma_\nu^2}\mathbf{Q}_\nu\mathbf{Q}_\nu^H\mathbf{Q}_\nu\mathbf{Q}_\nu^H\mathbf{u}_o}{\frac{1}{\sigma_\nu^2}\mathbf{u}_o^T\mathbf{Q}_\nu\mathbf{Q}_\nu^H\mathbf{Q}_\nu\mathbf{Q}_\nu^H\mathbf{u}_o} \\ &= \frac{\mathbf{Q}_\nu\mathbf{Q}_\nu^H\mathbf{u}_o}{\mathbf{u}_o^T\mathbf{Q}_\nu\mathbf{Q}_\nu^H\mathbf{u}_o}.\end{aligned} \tag{3.14}$$

Defining the ensemble-averaged autocorrelation matrix $\mathcal{R}$ of the received signal in eigen-decomposition terms, the MS at the output of the filter may be defined as follows:

$$\begin{aligned}\mathcal{J} = \mathbf{W}_{CM}^H\mathcal{R}\mathbf{W}_{CM} &= \mathbf{W}^H[\mathbf{Q}_I\Lambda_I\mathbf{Q}_I^H + \sigma_\nu^2\mathbf{Q}_\nu\mathbf{Q}_\nu^H]\mathbf{W} \\ &= \sigma_\nu^2\mathbf{W}^H\mathbf{Q}_\nu\mathbf{Q}_\nu^H\mathbf{W} \\ &= \frac{\sigma_\nu^2\mathbf{u}_o^T\mathbf{Q}_\nu\mathbf{Q}_\nu^H\mathbf{Q}_\nu\mathbf{Q}_\nu^H\mathbf{Q}_\nu\mathbf{Q}_\nu^H\mathbf{u}_o}{\|\mathbf{u}_o^T\mathbf{Q}_\nu\mathbf{Q}_\nu^H\mathbf{u}_o\|^2} \\ &= \frac{\sigma_\nu^2}{\mathbf{u}_o^T\mathbf{Q}_\nu\mathbf{Q}_\nu^H\mathbf{u}_o}.\end{aligned} \tag{3.15}$$

For a time-averaged autocorrelation matrix $\hat{\mathcal{R}}$:

$$\hat{\mathbf{W}}_{CM} = \frac{\hat{\mathcal{R}}^{-1}[I - \hat{\mathbf{Q}}_I\hat{\mathbf{Q}}_I^H]\mathbf{u}_o}{\mathbf{u}_o^T\hat{\mathcal{R}}^{-1}[I - \hat{\mathbf{Q}}_I\hat{\mathbf{Q}}_I^H]\mathbf{u}_o}. \tag{3.16}$$

Taking into account Equation 3.5, $\hat{\mathbf{W}}_{CM}$ may be re-written as follows:

$$\begin{aligned}\hat{\mathbf{W}}_{CM} &= \frac{[\hat{\mathbf{Q}}_I\hat{\Lambda}_I^{-1}\hat{\mathbf{Q}}_I^H + \hat{\mathbf{Q}}_\nu\hat{\Lambda}_\nu^{-1}\hat{\mathbf{Q}}_\nu^H]\hat{\mathbf{Q}}_\nu\hat{\mathbf{Q}}_\nu^H\mathbf{u}_o}{\mathbf{u}_o^T[\hat{\mathbf{Q}}_I\hat{\Lambda}_I^{-1}\hat{\mathbf{Q}}_I^H + \hat{\mathbf{Q}}_\nu\hat{\Lambda}_\nu^{-1}\hat{\mathbf{Q}}_\nu^H]\hat{\mathbf{Q}}_\nu\hat{\mathbf{Q}}_\nu^H\mathbf{u}_o} \\ &= \frac{\hat{\mathbf{Q}}_\nu\hat{\Lambda}_\nu^{-1}\hat{\mathbf{Q}}_\nu^H\mathbf{u}_o}{\mathbf{u}_o^T\hat{\mathbf{Q}}_\nu\hat{\Lambda}_\nu^{-1}\hat{\mathbf{Q}}_\nu^H\mathbf{u}_o}. \end{aligned} \tag{3.17}$$

Under highly negative SIR conditions, note that we have re-derived, in essence, the Wiener-Hopf filter given in Equation 3.11, with the additional constraint $\mathbf{W}^H\mathbf{Q}_I = \mathbf{0}$.

The normalized variances of the Wiener-Hopf and the Eigencanceler are derived in [9]. We performed some experiments evaluating the performance of the CMV filter against that of the Wiener-Hopf, and found both to yield similar results. Our conclusion is that the use of the eigenvalues, especially the noise eigenvalues, effects perturbation in the CMV filter on the same scale as in the Wiener-Hopf filter. In the interest of this work, then, we chose not to further pursue this venue.

3.3 Derivation of the Eigencanceler

Both the Wiener-Hopf and the CMV filters minimize the MSE term $\mathbf{W}^H\mathcal{R}\mathbf{W}$ at the output of the linear prediction filters. As a result, they attempt to cancel both the interference and the noise simultaneously, without the separation of one from the other. Due to measurement noise that arises from the use of a time-averaged autocorrelation matrix of the received signal, a solution may be found in separating the noise from the interference, then minimizing the power of the former while imposing an orthogonality constraint on the latter. This solution lies in using a *minimum norm* design, whereby the norm of the weight vector is minimized, as opposed to the MSE at the output of the filter. This design has been exploited in [6], [9] for the purposes of interference cancellation in array processing. We exploit the nature of the received signal in DS spread spectrum in the minimum norm design

in order to separate the noise from the interference, preserve the noise, namely the modulated data, *and* cancel the interference with robustness to measurement noise.

The minimum norm method is outlined from [10] here: Let the autocorrelation matrix of the signal be eigen-decomposed into two mutually orthogonal eigen-subspaces $\left[\mathbf{V}_I : \mathbf{V}_\nu\right]$, where the weight vector $\mathbf{C}$ has the following conditions imposed on it:

1. $\mathbf{C}$ lies in the range of $\mathbf{V}_\nu$. Hence,

$$\mathbf{C}^H \mathbf{V}_I = 0.$$

2. The first element of $\mathbf{C} = 1$. So,

$$\mathbf{C}^H \mathbf{u}_0 = 1$$

where $\mathbf{u}_o = [1\ 0 \ldots 0]$.

3. The Euclidean norm of $\mathbf{C}$, namely $\mathbf{C}^H\mathbf{C}$, is minimized, imposed with the two constraints specified above.

Instead of minimizing $\mathbf{W}^H \mathcal{R} \mathbf{W}$, the Eigencanceler will be derived by minimizing $\mathbf{W}^H\mathbf{W}$ with the constraints $\mathbf{W}^H\mathbf{u}_o = 1$ and $\mathbf{W}^H\mathbf{q}_I = 0$. Accordingly:

$$\zeta = \mathbf{W}^H\mathbf{W} + \lambda_1 \left(1 - \mathbf{W}^H\mathbf{u}_o\right) + \lambda_2 \left(-\mathbf{W}^H\mathbf{q}_I\right).$$

Minimizing the gradient with respect to $\mathbf{W}^H$,

$$\bigtriangledown\zeta = \mathbf{W} - \lambda_1\mathbf{u}_o - \lambda_2\mathbf{q}_I = 0.$$

Therefore,

$$\mathbf{W} = \lambda_1\mathbf{u}_o + \lambda_2\mathbf{q}_I.$$

The next step is to obtain the values for the two Lagrange multipliers, $[\lambda_1, \lambda_2]$. Applying the first constraint:

$$\begin{aligned} \mathbf{W}^H\mathbf{q}_I &= \lambda_1^*\mathbf{u}_o^T\mathbf{q}_I + \lambda_2^*\mathbf{q}_I^H\mathbf{q}_I = 0 \\ \therefore\ \lambda_2^* &= -\lambda_1^*\mathbf{u}_o^T\mathbf{q}_I. \end{aligned}$$

Applying the second constraint:

$$\begin{aligned}\mathbf{W}^H\mathbf{u}_o &= \lambda_1^*\mathbf{u}_o^T\mathbf{u}_o + \lambda_2^*\mathbf{q}_I^H\mathbf{u}_o \\ &= \lambda_1^*[1 - \mathbf{u}_o^T\mathbf{q}_I\mathbf{q}_I^H\mathbf{u}_o] = 1.\end{aligned}$$

Solving for $[\lambda_1, \lambda_2]$:

$$\begin{aligned}\lambda_1^* &= \frac{1}{1 - \mathbf{u}_o^T\mathbf{q}_I\mathbf{q}_I^H\mathbf{u}_o} \Rightarrow \lambda_1 = \frac{1}{1 - \mathbf{u}_o^T\mathbf{q}_I\mathbf{q}_I^H\mathbf{u}_o} \\ \lambda_2^* &= \frac{-\mathbf{u}_o^T\mathbf{q}_I}{1 - \mathbf{u}_o^T\mathbf{q}_I\mathbf{q}_I^H\mathbf{u}_o} \Rightarrow \lambda_2 = \frac{-\mathbf{q}_I^H\mathbf{u}_o}{1 - \mathbf{u}_o^T\mathbf{q}_I\mathbf{q}_I^H\mathbf{u}_o}.\end{aligned}$$

Solving for the weight vector:

$$\begin{aligned}\mathbf{W}_e &= \frac{[I - \mathbf{q}_I\mathbf{q}_I^H]\mathbf{u}_o}{\mathbf{u}_o^T[I - \mathbf{q}_I\mathbf{q}_I^H]\mathbf{u}_o} \\ &= \frac{\mathbf{Q}_\nu\mathbf{Q}_\nu^H\mathbf{u}_o}{\mathbf{u}_o^T\mathbf{Q}_\nu\mathbf{Q}_\nu^H\mathbf{u}_o}.\end{aligned} \tag{3.18}$$

The weight vector defined above meets the two specified constraints:

$$\begin{aligned}\mathbf{W}_e^H\mathbf{q}_I &= \frac{\mathbf{u}_o^T[1 - \mathbf{q}_I\mathbf{q}_I^H]\mathbf{q}_I}{1 - \mathbf{u}_o^T\mathbf{q}_I\mathbf{q}_I^H\mathbf{u}_o} = \frac{\mathbf{u}_o^T[\mathbf{q}_I - \mathbf{q}_I]}{1 - \mathbf{u}_o^T\mathbf{q}_I\mathbf{q}_I^H\mathbf{u}_o} = 0 \\ \mathbf{W}_e^H\mathbf{u}_o &= \frac{\mathbf{u}_o^T[1 - \mathbf{q}_I\mathbf{q}_I^H]\mathbf{u}_o}{1 - \mathbf{u}_o^T\mathbf{q}_I\mathbf{q}_I^H\mathbf{u}_o} = \frac{1 - \mathbf{u}_o^T\mathbf{q}_I\mathbf{q}_I^H\mathbf{u}_o}{1 - \mathbf{u}_o^T\mathbf{q}_I\mathbf{q}_I^H\mathbf{u}_o} = 1.\end{aligned}$$

The minimization of the term $\mathbf{W}^H\mathbf{W}$ is therefore given by:

$$\begin{aligned}\zeta_{min} = \mathbf{W}_e^H\mathbf{W}_e &= \frac{\mathbf{u}_o^T\mathbf{Q}_\nu\mathbf{Q}_\nu^H\mathbf{Q}_\nu\mathbf{Q}_\nu^H\mathbf{u}_o}{\|\mathbf{u}_o^T\mathbf{Q}_\nu\mathbf{Q}_\nu^H\mathbf{u}_o\|^2} \\ &= \frac{1}{\mathbf{u}_o^T\mathbf{Q}_\nu\mathbf{Q}_\nu^H\mathbf{u}_o}.\end{aligned} \tag{3.19}$$

The MS at the output of the filter is then given by,

$$\mathcal{J} \triangleq \mathbf{W}_e^H\mathcal{R}\mathbf{W}_e = \frac{\sigma_\nu^2}{\mathbf{u}_o^T\mathbf{Q}_\nu\mathbf{Q}_\nu^H\mathbf{u}_o}. \tag{3.20}$$

In a highly negative SIR environment with known signal statistics, it is noted that the Eigencanceler performs quasi-optimally in reference to the Wiener-Hopf, comparing the weight vectors in Equations 3.18 and 3.7, respectively, and the MS term $\mathcal{J}$ in Equations 3.20 and 3.8, respectively.

Given a time-averaged autocorrelation matrix, the Eigencanceler is given by:

$$\hat{\mathbf{W}}_e = \frac{\hat{\mathbf{Q}}_\nu \hat{\mathbf{Q}}_\nu^H \mathbf{u}_o}{\mathbf{u}_o^T \hat{\mathbf{Q}}_\nu \hat{\mathbf{Q}}_\nu^H \mathbf{u}_o}. \tag{3.21}$$

Using Equation 2.13 to test the robustness of the Eigencanceler to the measurement noise, the normalized variance of the Eigencanceler is given by [9]:

$$\mathrm{E}\left[\frac{\|\Delta \mathbf{W}_e\|^2}{\|\mathbf{W}_e\|^2}\right] = \frac{\lambda_{min}}{\lambda_{max}} \frac{1}{M}. \tag{3.22}$$

The perturbation of the Eigencanceler weight vector $\Delta \mathbf{W}_e \triangleq \hat{\mathbf{W}}_e - \mathbf{W}_e$, is smaller than that of the Wiener-Hopf weight vector by a factor of the inverse of the eigenvalue-spread. No eigenvalues are used and the noise eigenvectors are normalized; hence, there is no large-scale fluctuation in the formation of the tap-weights, as evidenced in Equation 3.22. In contrast, the Wiener-Hopf exhibits strong sensitivity to fluctuations in noise eigenvalues, as illustrated in Equation 3.12.

CHAPTER 4

THE EIGENCANCELER ALGORITHM

Chapter 3 focuses on the derivation of the Eigencanceler using blocks of data to estimate the autocorrelation matrix and subsequently derive the weight vector. This chapter deals with the development of the recursive Eigencanceler algorithm, using the classical power method to extract the eigenvectors corresponding to the largest eigenvalues in descending order [5].

The algorithm is developed as follows:

The parameters are initialized:

$$\begin{aligned} \hat{\mathcal{R}}_0 &= \mathbf{I} + \mathbf{U}_0\mathbf{U}_0^T, \\ \mathbf{q}_0 &= [1\ 0 \ldots 0]^T \\ \mathcal{P}^{(1)} &= I \end{aligned}$$

where $\mathbf{U}_0$ is the first set of received signal samples, q_0 is an initializing vector. $\mathcal{P}^{(l)}$ is a projection matrix, designed to maintain the orthogonality between each eigenvector, by projecting the l-th eigenvector in a subspace orthogonal to all the previously derived $(l-1)$ eigenvectors.

The following steps will derive the eigenvectors corresponding to the largest eigenvalues in $\hat{\mathcal{R}}_k$:

1. The i-th iteration at time k of the l-th eigenvector:

$$\begin{aligned} V_{k,i+1}^{(l)} &= \mathcal{P}^{(l)}\hat{\mathcal{R}}_k\mathbf{q}_k^{(l)} \\ \mathbf{q}_k^{(l)} &= \frac{V_{k,i+1}^{(l)}}{\|V_{k,i+1}^{(l)}\|} \end{aligned}$$

where $\mathcal{P}^{(l)}$ is the projection matrix. Note: Step 2 is run 2-3 times for accurate derivation of the eigenvectors.

2. The projection matrix is updated:

$$P^{(l+1)} = P^{(l)} - \mathbf{q}_k^{(l)}\mathbf{q}_k^{(l)T}$$

3. Steps 2-3 are repeated until all interference eigenvectors have been resolved into an interference subspace $\mathbf{Q}_{I,k} \triangleq \mathrm{E}[\mathbf{q}_1 \ldots \mathbf{q}_p]$, where $p < M$ is the number of degrees of freedom assigned to the interference subspace.

4. The weight vector is updated:

$$\mathbf{W}_{e,k+1} = \alpha[I - \mathbf{Q}_{I,k}\mathbf{Q}_{I,k}^T]\mathbf{u}_o \tag{4.1}$$

where $\alpha = (\mathbf{u}_o^T[I - \mathbf{Q}_{I,k}\mathbf{Q}_{I,k}^T]\mathbf{u}_o)^{-1}$.

5. The estimate of the autocorrelation matrix given by [14]:

$$\hat{\mathcal{R}}_k = \left(1 - \frac{1}{k}\right)\hat{\mathcal{R}}_{k-1} + \frac{1}{k}\mathbf{U}_k\mathbf{U}_k^T \tag{4.2}$$

The Eigencanceler algorithm is evaluated in its convergence rate to the Eigencanceler formed under known signal statistics and in the convergence rate of the MS at the output of the filter. Given a case where the interference is tone modeled as a complex exponential, it occupies only one degree of freedom.

Proceeding in a manner similar to that expressed in [7], to simplify the analysis of the rate of convergence of the adaptive Eigencanceler we will consider the case that the interference subspace $\mathbf{Q}_I = \left[\mathbf{q}^{(1)}\right]$, i.e., it consists of a single eigenvector (this is true for a tone interference represented by a complex exponential). For brevity of notation let $q = q^{(1)}$. The Eigencanceler's weight vector at the k-th iteration is given, up to scaling factor, by: $\mathbf{W}_k = \left(\mathbf{I} - \mathbf{q}_k\mathbf{q}_k^T\right)\mathbf{u}_o$. Then, the weight vector error is expressed by:

$$\begin{aligned} \varepsilon_k &= \mathbf{W}_k - \mathbf{W}_e \\ &= \left(\mathbf{q}^T\mathbf{u}_o\right)\mathbf{q} - (\mathbf{q}_k^T\mathbf{u}_o)\mathbf{q}_k \end{aligned} \tag{4.3}$$

The eigenvector $\mathbf{q}_k$ is estimated using the power method. We wish to focus on the speed of convergence due to the estimation of eigenvectors. Consequently, we will

assume that the correlation matrix $\hat{\mathcal{R}}_k$ has converged to $\mathcal{R}$. The initial estimate of $\mathbf{q}$ can be expressed in the basis formed by all the eigenvectors of $\mathcal{R}$:

$$\mathbf{q}_o = \alpha_1 \mathbf{q} + \alpha_2 \mathbf{q}^{(2)} \ldots + \alpha_M \mathbf{q}^{(M)}. \tag{4.4}$$

At the k-th iteration of the power method we have:

$$\begin{aligned} \mathbf{q}_k &= c_1^k \mathcal{R}^k \mathbf{q}_o \\ &= c_1 \alpha_1 \lambda_1^k \left(\mathbf{q} + \sum_{\ell=2}^{M} \frac{\alpha_\ell}{\alpha_1} \left(\frac{\lambda_\ell}{\lambda_1} \right)^k \mathbf{q}^{(\ell)} \right). \end{aligned} \tag{4.5}$$

If c_1 is chosen such that $c_1 \alpha_1 \lambda_1^k = 1$, then we can express $\mathbf{q}_k$ as the sum of two orthogonal vectors: $\mathbf{q}_k = \mathbf{q} + \mathbf{b}_k$. Using this relation in Equation 4.3 results in

$$\varepsilon_k = -\left[\left(\mathbf{q}^T \mathbf{u}_o \right) \mathbf{b}_k + \left(\mathbf{b}_k^T \mathbf{u}_o \right) \mathbf{q} + \left(\mathbf{b}_k^T \mathbf{u}_o \right) \mathbf{b}_k \right]. \tag{4.6}$$

Exploiting the orthogonality between $\mathbf{q}$ and $\mathbf{b}_k$, and the relation $\mathbf{q}^T \mathbf{q} = 1$, we get:

$$\|\varepsilon_k\|^2 = \left(\mathbf{b}_k^T \mathbf{u}_o \right)^2 + \left(\mathbf{q}^T \mathbf{u}_o \right)^2 \|\mathbf{b}_k\|^2. \tag{4.7}$$

From Equation 4.5 it can be observed that this term decays as fast as $(\lambda_2/\lambda_1)^2$. Hence we have,

$$\|\varepsilon_{k+1}\|^2 \simeq \left(\frac{\lambda_2}{\lambda_1} \right)^2 \|\varepsilon_k\|^2. \tag{4.8}$$

For a strong interference the adaptive Eigencanceler will converge faster than either the LMS or RLS algorithms.

Assuming the same initial conditions given for the LMS and the RLS, the convergence rate of $\mathbf{W}_{e,k}$ to $\mathbf{W}_e$ at time k may be expressed by:

$$\mathrm{E}\left[\|\varepsilon_k\|^2 \right] \simeq \left(\frac{\lambda_2}{\lambda_1} \right)^{2k} \mathrm{E}\left[\|\mathbf{W}_e\|^2 \right]. \tag{4.9}$$

Comparing Equations 2.21 and 2.28 to 4.9, it is duly noted that the Eigencanceler algorithm converges to *its* optimal solution faster than do the LMS and the RLS to the Wiener-Hopf. It is also noted that the larger the interference power, the faster the convergence of the Eigencanceler algorithm to its optimal solution.

The MS at the output of the filter is given by Equation 2.21, re-written here:

$$\mathcal{J}(k) = \mathcal{J}'_{min} + \sigma_u^2 \mathrm{E}\left[\|\varepsilon_k\|^2\right] \tag{4.10}$$

where $\mathcal{J}'_{min}$ is the minimum MS attained by the Eigencanceler at the output of the filter, under known signal statistics. Combining Equations 4.9 and 4.10, the MS at the output of the filter may be expressed as:

$$\begin{aligned}\mathcal{J}(k) &= \mathcal{J}'_{min} + \sigma_u^2 \left(\frac{\lambda_2}{\lambda_1}\right)^{2k} \mathrm{E}\left[\|\mathbf{W}_e\|^2\right] \\ &= \mathcal{J}_{min} + \frac{\mathbf{u}_o^T \mathcal{R}_I^{-1} \mathbf{u}_o}{\|\mathbf{u}_o^T \mathcal{R}_\nu^{-1} \mathbf{u}_o\|^2} + \sigma_u^2 \left(\frac{\lambda_2}{\lambda_1}\right)^{2k} \mathrm{E}\left[\|\mathbf{W}_e\|^2\right].\end{aligned} \tag{4.11}$$

where $\mathcal{J}_{min}$ is the minimum MS at the output of the filter achieved by the Wiener-Hopf filter under known signal statistics. $\mathcal{R}_I^{-1}$ and $\mathcal{R}_\nu^{-1}$ are the inverse of the ensemble-averaged autocorrelation matrices of the interference and noise, respectively.

Under highly negative SIR conditions, the second term in Equation 4.11 converges to zero, in effect. Therefore, comparing the MS at the k-th iteration due to the LMS and the RLS in Equations 2.21 and 2.28, respectively, to Equation 4.11, the Eigencanceler algorithm minimizes the MS at the output of the filter within far fewer iterations than either the LMS or the RLS.

A final note on the practical consideration of the Eigencanceler algorithm: The LMS is well known to have order M complexity ($\mathcal{O}(M)$), whereas the RLS has $\mathcal{O}(M^2)$ complexity. Since the Eigencanceler algorithm involves the multiplication of matrices upto $M \times M$, the Eigencanceler has order $\mathcal{O}(M^2)$ complexity [6]. In summary, the Eigencanceler proves to converge faster than the LMS and the RLS, even with an order $\mathcal{O}(M^2)$ complexity.

CHAPTER 5

PERFORMANCE ANALYSIS

5.1 Eigenanalysis

In Chapter 3, the received data is represented in terms of the eigenvalues and eigenvectors of its autocorrelation matrix. We noted that the narrow-band interference occupies a few degrees of freedom in the signal eigen-space, marked by a few large eigenvalues. This section will cover the number of degrees of freedom to be assigned to the interference subspace, i.e., the number of eigenvalues which are to be termed interference eigenvalues.

The eigenvalue decomposition of the correlation matrix of the received data reveals several interesting properties. Proceeding in a manner similar to that expressed in [8], consider $\mathcal{R}_I$, the correlation matrix of the interference contributions present in the filter structure. For a tone interference, $\mathcal{R}_I = \mathrm{E}\left[\mathrm{j}_k\, \mathrm{j}_k^T\right]$, where the expectation operation is over the random initial phase θ. Dropping the time subscript for brevity, $\mathrm{j}^T = [\cos\theta,\ \cos(\omega T_c + \theta) \cdots,\ \cos(\omega(M-1)T_c + \theta)]$. The interference vector can be expressed using the complex vectors $\mathrm{j} = \frac{1}{2}\left(e^{j\theta}\mathrm{f} + e^{-j\theta}\mathrm{f}^*\right)$, $\mathrm{f}^T = \left[1,\ e^{j\omega T_c} \cdots,\ e^{j\omega(M-1)T_c}\right]$. Using these definitions, we have $\mathcal{R}_I = \frac{1}{4}\left(\mathrm{f}\ \mathrm{f}^H + \mathrm{f}^*\mathrm{f}^T\right)$. Since f and f^* are linearly independent, it follows that the interference correlation matrix, which is the sum of two rank one matrices, has rank two, i.e., only two non-zero eigenvalues. The eigenvalues of the data matrix $\mathcal{R}$ are determined by the combination of spread spectrum data, interference and thermal noise. The data and thermal noise are assumed white, and their effect is to add a constant level $(S + \sigma_n^2)$ to all the eigenvalues of $\mathcal{R}_I$. Consequently, the energy contributed by a tone interference is concentrated in the two largest eigenvalues of the correlation matrix $\mathcal{R}$.

As the bandwidth of the interference is increased, the number of eigenvalues in which most of the interference energy is contained is predicted by the Landau-Pollak theorem and is equal to,

$$N = 2B\tau + 1 \tag{5.1}$$

where B is the interference bandwidth and τ is its duration across the filter structure [23]. In the extreme wide-band case, the bandwidth is equal to half the sampling rate, $B_{SS} = 1 \,/\, 2T_c$, and since $\tau = (M-1)\,T_c$, $N = M$. Thus, the interference energy is spread across all the system eigenvalues. When the interference occupies only part of the bandwidth, $B = \Delta \,/\, 2T_c$, where Δ is the fractional bandwidth with respect to B_{SS}, and the number of interference contributed eigenvalues is $N = \Delta\,(M-1)+1 \leq M$. The above analysis guarantees that the filter will utilize the smallest number of degrees of freedom required to reject the interference.

In this work, we will assign a filter length of $M = 5$ for a tone interference and $M = 15$ for a narrow-band Gaussian interference. Accordingly, the number of dominant eigenvalues predicted by the Landau-Pollak theorem for narrow-band Gaussian interference with fractional bandwidth $\Delta = 0.1$ is $N = 0.1\,(15-1)+1 = 2.4 \cong 3$.

Figure 5.1 depicts the eigenvalues of the ensemble-averaged autocorrelation matrices of the received signal, for both types of interference, each computed with two different SIR ratios, namely, SIR = -10 dB and SIR = -20 dB. While it ascertains the number of degrees of freedom assigned to a tone interference, it marks an additional significant eigenvalue for the narrow-band Gaussian interference with a fractional bandwidth of 0.1, making $N = 4$. We note that the Landau-Pollak theorem offers an approximation of the number of significant eigenvalues contained in the signal autocorrelation matrix. We also note that the number of significant eigenvalues predicted by the theorem becomes more accurate for the case where the time-bandwidth product $B\tau$ is large, which is *not* our case. Therefore, we chose to

use the simulation results as a rule of thumb. We thus assign $N = 4$ significant eigenvalues to the narrow-band interference.

The question arises as to whether the actual number of significant eigenvalues which determines the number of eigenvectors to be included in the interference subspace is affected by the interference power in addition to the interference bandwidth. We will look at two cases where SIR = -10 dB and SIR = -20 dB. It is well known that increasing the power of the interference by a factor of 10 also increments only the interference eigenvalues by a factor of 10, evidenced by the increment in the trace of the autocorrelation matrix of the received signal [10], as depicted in Figure 5.2. Therefore, the interference eigenvalues corresponding to an SIR = -20 dB are larger than the interference eigenvalues corresponding to an SIR = -10 dB by a factor of 10.

One way of looking at the problem is to calculate/simulate the percentage of the total power contained in each eigenvalue, most of which is attributed to the interference. The percentage of the total power of the received signal in each eigenvalue is determined by dividing the sum of all other successive eigenvalues by the trace of the autocorrelation matrix of the received signal. Figure 5.3 confirms that most of power of the received signal, which is credited to the interference, lies in the first few eigenvalues. In addition, it shows that the percentage of power in each eigenvalue is not significantly altered by the change in SIR from -10 dB to -20 dB. In fact, when the interference power is incremented, the trace of the autocorrelation matrix is incremented as well; hence, although the eigenvalue spread is larger, the power is distributed more evenly over the entire eigenspace. Therefore, decreasing the SIR to -20 dB does not require that N be changed.

Another way of looking at the problem is to evaluate the system performance of the Eigencanceler by varying N. We will determine whether increasing the value of N improves the system performance, noting that the sidelobes of the interference

increase in proportion to increase in the interference power. We use values of $N = 4$ and $N = 5$ for both cases of SIR in the Eigencanceler and evaluate it in the probability of error. As depicted in Figure 5.4, changing N for both SIR's does not significantly improve the system performance. Although we note that for an SIR of -10 dB, $N = 4$ yields a lower probability of error and that for an SIR of -20 dB, $N = 5$ yields a lower probability of error, the improvements in themselves are not significant enough to implement them throughout the work. Therefore, in keeping with the original intent of letting $N = 4$ for all SIR, we will evaluate the figures of merit on the Eigencanceler method and algorithm in the following sections.

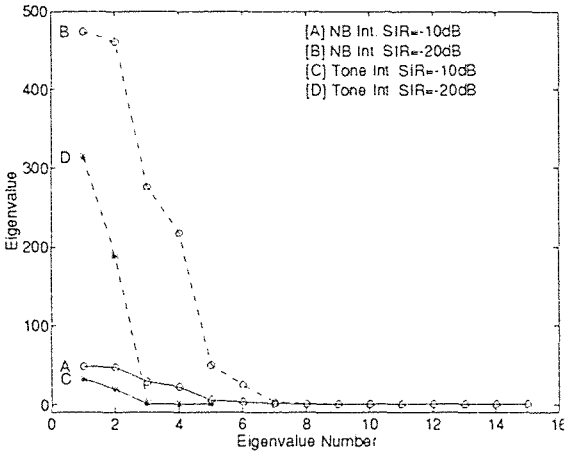

Figure 5.1 Eigenvalues of theoretical sample covariance matrix.

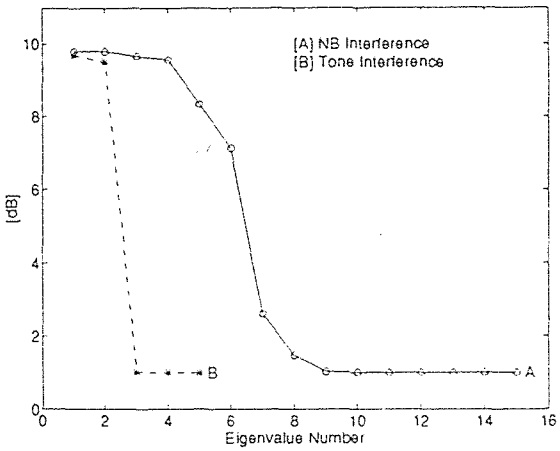

Figure 5.2 Ratio of eigenvalues vs. eigenvalue number.

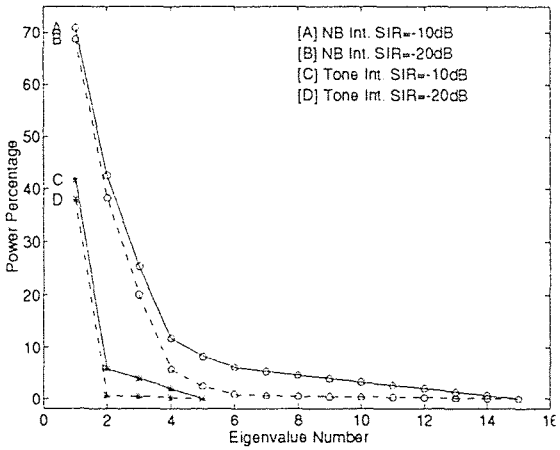

Figure 5.3 Percentage of power contained in each eigenvalue vs. eigenvalue number.

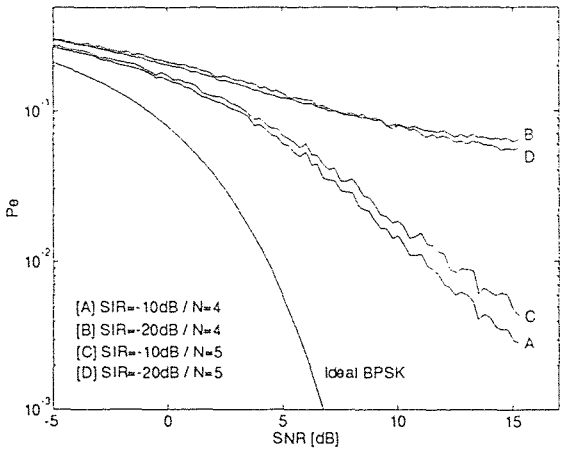

Figure 5.4 Probability of error vs. SNR for Eigencanceler for narrow-band interference.

5.2 Performance of the Block Eigencanceler vs. the Wiener-Hopf

The block Wiener-Hopf and Eigencanceler are evaluated in the normalized variance of the weight vector, in the improvement in SNIR η, and in the probability of error P_e.

The normalized variance of the weight vector is given by Equation 2.13, rewritten here for convenience:

$$\mathrm{E}\left[\frac{||\Delta \mathbf{W}||^2}{||\mathbf{W}||^2}\right]$$

where $\Delta \mathbf{W} = \hat{\mathbf{W}} - \mathbf{W}$, $\mathbf{W}$ is the optimal weight vector, and $\hat{\mathbf{W}}$ is the weight vector based on the estimate of the autocorrelation matrix of the received signal.

The improvement in SNIR is given by Equations 2.8 and 2.9,

$$\eta \;=\; L\,\frac{J+\sigma_n^2}{\mathbf{W}^H\mathcal{R}_I\mathbf{W} + (\sigma_n^2+1)\mathbf{W}^H\mathbf{W} - 1}$$

The probability of error is given by Equation 2.10, also rewritten here for convenience:

$$P_e \;=\; \mathcal{Q}\left(\sqrt{\mathrm{SNIR}_{out}}\right)$$

where $\mathcal{Q}(x) \;\triangleq\; 0.5\ \mathrm{erfc}\left(x/\sqrt{2}\right)$.

The following simulations are created using Matlab 4.0 on a Sun Workstation. The chief factors considered in the comparison of the performances of the Eigencanceler and the Wiener-Hopf are listed below:

1. The number of iterations or samples of the received signal;

2. The SIR and SNR in [dB];

3. The length of the interference-suppressant FIR filter.

5.2.1 Normalized Variance of the Weight Vectors

This section considers the perturbation effected by the measurement noise in the weight vectors for the Wiener-Hopf and Eigencanceler filters. The normalized variance of the weight vectors, given by Equation 2.13, is plotted against the size K of the data block used in estimating the autocorrelation matrix $\hat{\mathcal{R}}$, and subsequently in creating the weight vector estimate $\hat{\mathbf{W}}$. The optimal weight vector is determined in the case where the signal statistics are known, and accordingly, the Wiener-Hopf and the Eigencanceler weight vectors are computed. Two cases are shown: tone interference and narrow-band Gaussian intereference. The filters are tested using SIR = -10 dB and SIR = -20 dB for both types of interference, with a constant SNR = 10 dB. Again, the filter length for the tone interference case is $M = 5$ whereas for the narrow-band interference case, $M = 15$. To maintain the non-singularity of the autocorrelation matrix, we assign a minimum block size of $K = 5^2 = 25$ to the tone interference, and likewise, $K = 15^2 = 225$ to the narrow-band interference. We also assign multiples of those blocks, namely $K = 50, 75, 100,$ and 125 to the tone interference. Likewise, we assign $K = 450, 675, 900,$ and 1125 to the narrow-band interference.

Table 5.1 Normalized variances of weight vectors for tone interference

	SIR = -10 dB		SIR = -20 dB	
K	WH	EC	WH	EC
25	6.2	0.0314	0.3324	0.0021
50	0.3668	0.0153	0.2392	0.0012
75	0.1695	0.0102	0.3597	0.0009
100	0.1173	0.0076	0.2227	0.0007
125	0.0827	0.0061	0.1616	0.0006

Table 5.1 shows that with as few as $K = 25$ samples for the tone interference, the variance of the Eigencanceler (EC) is 0.0314 and 0.0021, for SIR = -10 dB and SIR = -20 dB, respectively. In comparison, for the Wiener-Hopf (WH), the variance

Table 5.2 Normalized variances of weight vectors for narrow-band interference

	SIR = -10 dB		SIR = -20 dB	
K	WH	EC	WH	EC
225	78.10	0.0902	0.1795	0.0077
450	0.7202	0.0358	0.1672	0.0047
675	0.3526	0.0225	0.1535	0.0035
900	0.2382	0.0156	0.1485	0.0027
1125	0.1772	0.0123	0.1663	0.0022

is 6.2 and 0.3324, for SIR = -10 dB and SIR = -20 dB, respectively. Similarly, Table 5.2 shows that with as few as $K = 225$ samples, the Eigencanceler is shown to have a much lower normalized variance than the Wiener-Hopf. Both tables reveal that the variance of the Eigencanceler is decreased approximately by a factor of 10 from an SIR = -10 dB to an SIR = -20 dB. This is explained by Equation 3.22 for the normalized variance weight vector of the Eigencanceler, in which the variance is inversely proportional to the eigenvalue spread. Therefore, the greater the spread, the lower the variance. In contrast, for the Wiener-Hopf the variances do not change as drastically. The exception are the cases where $K = 25$ for the tone interference and $K = 225$ for the the narrow-band interference, both for the SIR = -10 dB. These values of K are the minimum size that may be collected for obtaining a full rank autocorrelation matrix. The noise perturbation is significant at this level, so it adversely affects the function of the Wiener-Hopf for an SIR = -10 dB. This is not the case, however, for an SIR = -20 dB. Since the interference power is sufficiently high, the noise perturbation is less effective. The Eigencanceler, due to its insensitivity to noise perturbation, may take advantage of the minimum required size of the data block to estimate and excise the interference.

We plot the normalized variance of the weight vector as a function of the size of the block of data K to show how the perturbance is effected in the Wiener-Hopf and in the Eigencanceler as a function of K. Figure 5.5 depicts the normalized variance

of the weight vector simulations for the Eigencanceler and the Wiener-Hopf. The normalized variances of the weight vectors are plotted as a function of the size of the data block, given a tone interference and a narrow-band Gaussian interference.

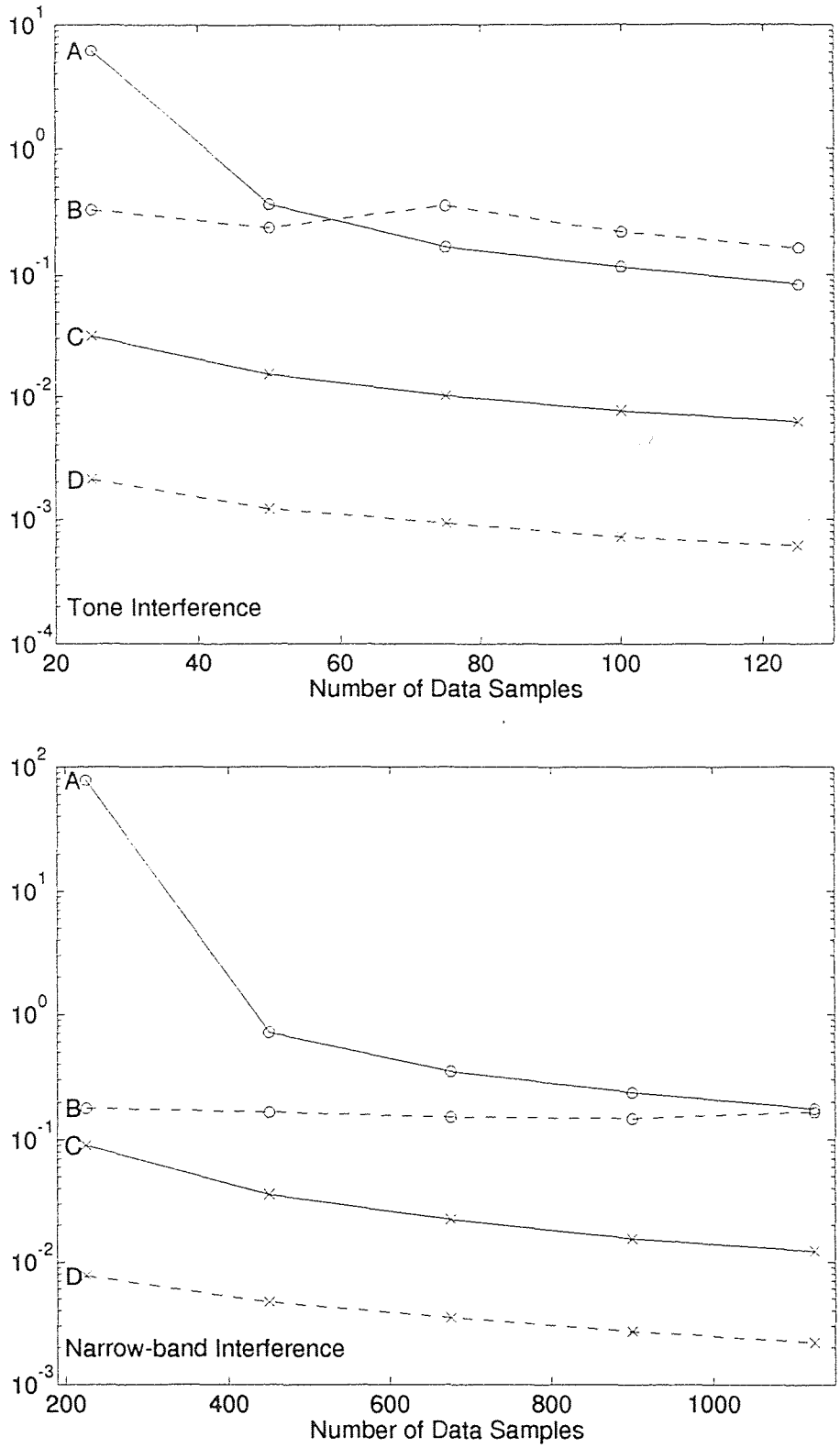

Figure 5.5 Normalized variance of weight vectors vs. size of data block
[A]Wiener-Hopf (SIR = -10 dB) [B]Wiener-Hopf (SIR = -20 dB)
[C]Eigencanceler (SIR = -10 dB) [D]Eigencanceler (SIR = -20 dB)

Another way of showing the convergence of the weight vectors to their optimal solution is to simulate the frequency response plots of the weight vectors. The frequency response plots for the case of a tone interference do not reveal much information; hence, we chose not to include nor discuss the frequency response plots for a tone interference. Accordingly, we generated four sets of plots for the case of a narrow-band Gaussian interference. Each plot depicts the frequency response of the Eigencanceler and the Wiener-Hopf filters. We include the bandwidth occupied by the interference in order to illustrate graphically the effectiveness of the *notch* created by the filter in the region. The simulations are generated for cases where the signal statistics are both known and unknown. For the unknown cases, we ran 1000 independent tests and averaged the resulting weight vectors for the Eigencanceler and the Wiener-Hopf filters. We used blocks of data of size $K = 225$ for SIR = -10 dB and for SIR = -20 dB. The simulations agree well with the results presented in Table 5.2.

We note that as the SIR is decreased from -10 dB to -20 dB, the third and fourth plots in Figure 5.6 show a deepening of the notch. The second plot shows that the Eigencanceler and Wiener-Hopf weight vectors are closer in shape than the fourth plot. This seemingly does *not* corroborate the statement made in Chapter 3 to the effect that as the interference power is increased, the Wiener-Hopf approaches the Eigencanceler. This is verified numerically by comparing the normalized squared difference between the Eigencanceler and the Wiener-Hopf weights in a *known* signal environment, i.e.,

$$\mathrm{E}\left[\frac{\|\mathbf{W}_e - \mathbf{W}_o\|^2}{\|\mathbf{W}_o\|^2}\right].$$

For SIR = -10 dB, the normalized squared difference is 0.2838. Whereas, for SIR = -20 dB, the normalized squared difference is at 0.5551 almost twice that for SIR = -10 dB.

The explanation lies in the use of narrow-band interference with *finite* bandwidth as opposed to a tone interference with *zero* bandwidth. The interference energy in former is not *completely* contained within the prescribed number of degrees of freedom given to the interference subspace. There is residual interference energy residing in the noise subspace occupied by the weight vector for the Eigencanceler. This is *more* pronounced for a highly negative SIR. The statement made in Chapter 3 holds for an interference whose energy is *entirely* contained in the prescribed number of degrees of freedom given to the interference subspace, e.g., the tone interference whose *entire* energy is contained in the first two eigenvalues of the ensemble-averaged autocorrelation matrix of the received signal. However, this does not detract from the performance of the Eigencanceler, because the frequency response plots show that in an unknown signal environment, the Eigencanceler offers virtually the same *depth* in the notch in the interference bandwidth area. In addition, the Eigencanceler has lower sidelobes, in general, indicating its robustness to measurement noise, in contrast to the Wiener-Hopf filter.

In summary, these results show that the Eigencanceler converges to its optimal solution, which, though sub-optimal to the Wiener-Hopf in a known environment, will prove to be superior to the Wiener-Hopf in an unknown environment. Because of this insensitivity to perturbation, in the following sections the Eigencanceler will prove to offer superior performance given few data .

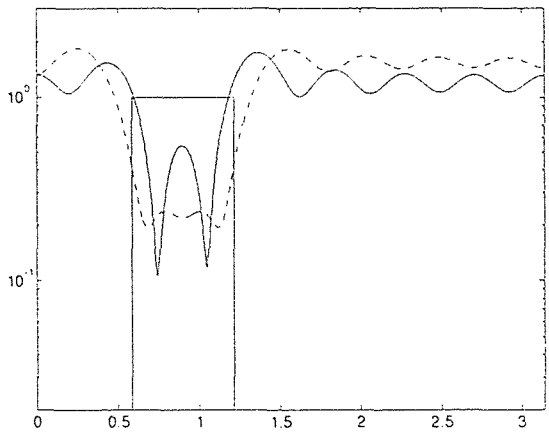

Frequency response of weight vectors for **known** signal statistics (SIR = -10 dB).

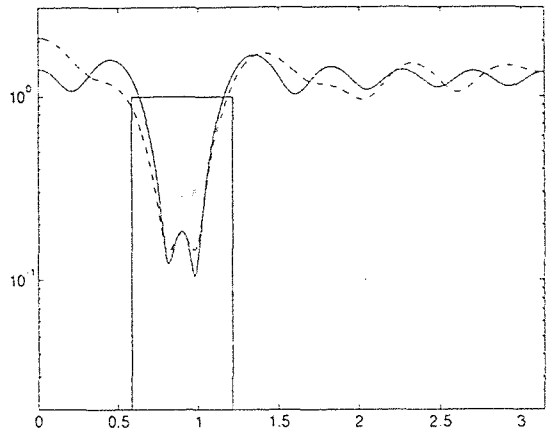

Frequency response of weight vectors for **unknown** signal statistics (SIR = -10 dB).

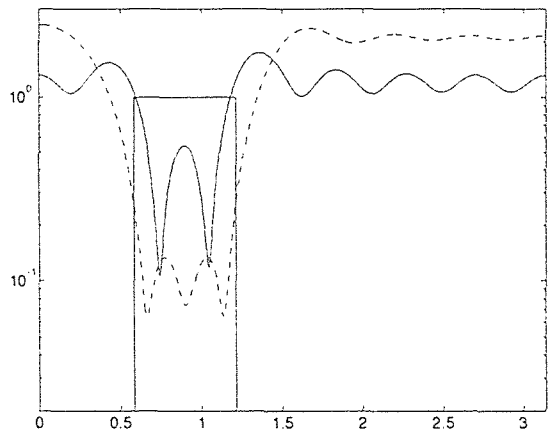

Frequency response of weight vectors for **known** signal statistics (SIR = -20 dB).

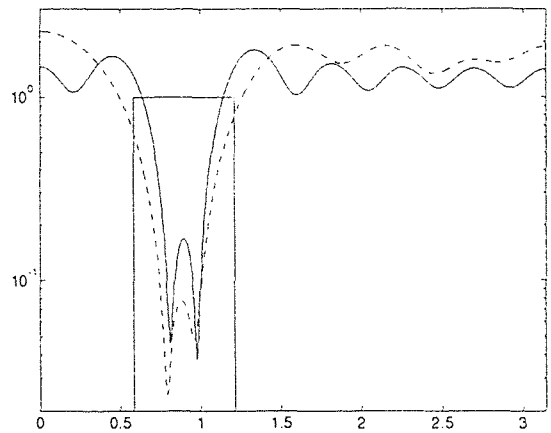

Frequency response of weight vectors for **unknown** signal statistics (SIR = -20 dB).

Figure 5.6 Frequency response plots of weight vectors for narrow-band interference [Solid] Eigencanceler [Dashed] Wiener-Hopf.

5.2.2 SNIR Improvement Factor

The improvement in the SNIR expresses the physical amount of interference power excised from the received signal. In Chapters 1 and 2, we discussed the fixed matched filter which offers a fixed processing gain. Therefore, any residual interference exiting the adaptive interference suppressant filter is suppressed to the extent of the processing gain L. We implement a processing gain of $L = 10\log_{10}(15) = 11.7$ dB. Any residual interference-plus-noise power will mask the desired signal; hence, the implementation of adaptive interference-suppressant filters.

We will evaluate the performance of the Eigencanceler and the Wiener-Hopf by calculating the improvement in SNIR at the output of the PN demodulator as a function of the SNIR at the input of the receiver. The tables for the tone and narrow-band interferences show the gain offered by the adaptive filters at various data block sizes K at SIR = -10 dB and at SIR = -20 dB. They also show the difference in the gains offered by the filters.

Table 5.3 SNIR improvement offered by adaptive filters vs. input SNIR for tone interference.

	$SNIR_{in}$	Gain [dB]		Difference	$SNIR_{in}$	Gain [dB]		Difference
K	[dB]	WH	EC	EC-WH	[dB]	WH	EC	EC-WH
25	-20	7.1	9.5	2.4	-10	3.5	6.9	3.4
50	-20	11.5	12.2	0.65	-10	7.5	8.6	1.1
75	-20	13.3	13.7	0.42	-10	8.7	9.3	0.63
100	-20	14.4	14.8	0.37	-10	9.6	9.9	0.30
125	-20	15.2	15.6	0.35	-10	9.9	10.2	0.28

In the case of the tone interference, the Eigencanceler, by itself, offers a received signal with an input SNIR of -20 dB an advantage of 9.5 dB at $K = 25$. In combination with $L = 11.76$ dB, the SNIR at the output of the filter is 1.26 dB, an improvement of 21.26 dB. Likewise, for the narrow-band interference, a signal received with an input SNIR of -20 dB is offered a gain of 12.0 dB at $K = 225$ if processed by the

Table 5.4 SNIR improvement offered by adaptive filters vs. input SNIR for narrow-band interference.

K	$SNIR_{in}$	Gain [dB]		Difference	$SNIR_{in}$	Gain [dB]		Difference
	[dB]	WH	EC	EC-WH	[dB]	WH	EC	EC-WH
225	-20	5.1	12.0	6.9	-10	-0.89	7.7	8.6
450	-20	13.3	13.1	-0.16	-10	6.3	8.6	2.3
675	-20	14.5	13.4	-1.1	-10	7.7	9.1	1.4
900	-20	15.2	13.5	-1.6	-10	8.4	9.2	0.85
1125	-20	15.5	13.5	-2.0	-10	8.8	9.3	0.52

Eigencanceler. In combination with $L = 11.76$ dB, the received signal has an SNIR at the output of the filter of 3.76 dB, which is an improvement of 23.76 dB.

The Wiener-Hopf, however, offers a gain of 7.1 dB under the same conditions for a tone interference and 5.1 dB for a narrow-band interference. These figures result in an SNIR at the output of the PN demodulator of -1.14 dB and -3.14 dB, respectively. Therefore, the desired signal will remain masked by the interference and noise based on $K = 25$ and $K = 225$ for the tone and narrow-band interferences, respectively.

At $K = 25$, from $SNIR_{in}$ = -4.4 to 0 dB, the Wiener-Hopf adversely affects the desired signal, by lowering the SNIR ratio at the output of the adaptive filter by factors ranging from -0.0577 dB to -3.7615 dB. Doubling the data size to $K = 50$ improves the system performance offered by the Wiener-Hopf such that it offers a positive advantage to the desired signal.

Likewise, for a narrow-band interference, at $K = 225$, the Wiener-Hopf decreases the SNIR by factors ranging from -0.1509 dB to -9.7418 dB, for SNIR at the input ranging from -11.5264 dB to 0 dB. At this point, it is preferable to use the fixed matched filter alone to offer a processing gain of $L = 11.76$ dB. In this case, the SNIR at the output of the filter is positive for the input SNIR range specified above. The performance of the Wiener-Hopf improves when the number of samples

is doubled to $K = 450$, where the Wiener-Hopf adversely affects the desired signal with negative processing gains ranging from -0.5299 dB to -1.644 dB for input SNIR ranging from -1.793 dB to 0 dB.

Five plots, depicted in Figure 5.7, are based on the size of the data blocks. For the tone interference, the first plot in Figure 5.7 illustrates the superior performance of the Eigencanceler over the Wiener-Hopf with the minimum required size of data blocks of $K = 25$. The third plot in Figure 5.7, corresponding to $K = 75$, shows that after an input SNIR ranging from -3.9253 to 0 dB, the Wiener-Hopf improves in performance and offers upto an 0.8318 dB improvement in gain over the Eigencanceler at input SNIR = 0 dB. As the number of samples increases, the Wiener-Hopf edges close to the Eigencanceler in SNIR, and surpasses it in the low interference plus noise power region.

For the case of the narrow-band interference, at $K = 225$, the Eigencanceler clearly demonstrates superior performance over the Wiener-Hopf, as depicted in the first plot in Figure 5.8. A notable difference between the results for this interference and the tone interference is that in the highly negative SIR region, the Wiener-Hopf surpasses the Eigencanceler for values of K greater than 675, inclusive.

All simulations reveal that the SNIR improvement factor of the Eigencanceler converges to its optimal performance given a minimum size of data block. An increase in the number of iterations does not improve the system performance of the Eigencanceler to the extent that the Wiener-Hopf is affected. The effect of the number of data employed on the performance of the Wiener-Hopf indicates its sensitivity to noise perturbation, as opposed to the Eigencanceler.

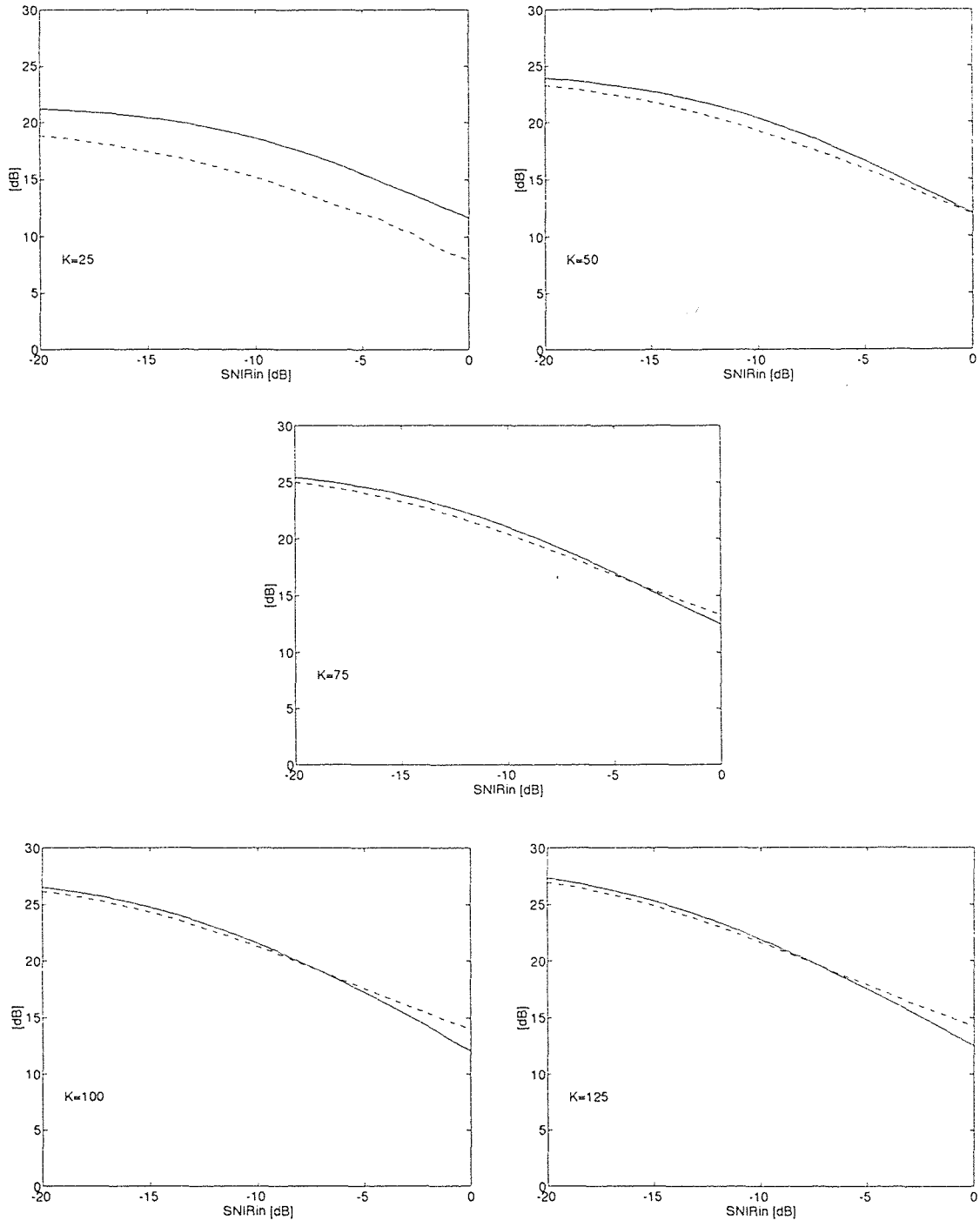

Figure 5.7 SNIR improvement factor vs. input SNIR for tone interference [Solid] Eigencanceler [Dashed] Wiener-Hopf.

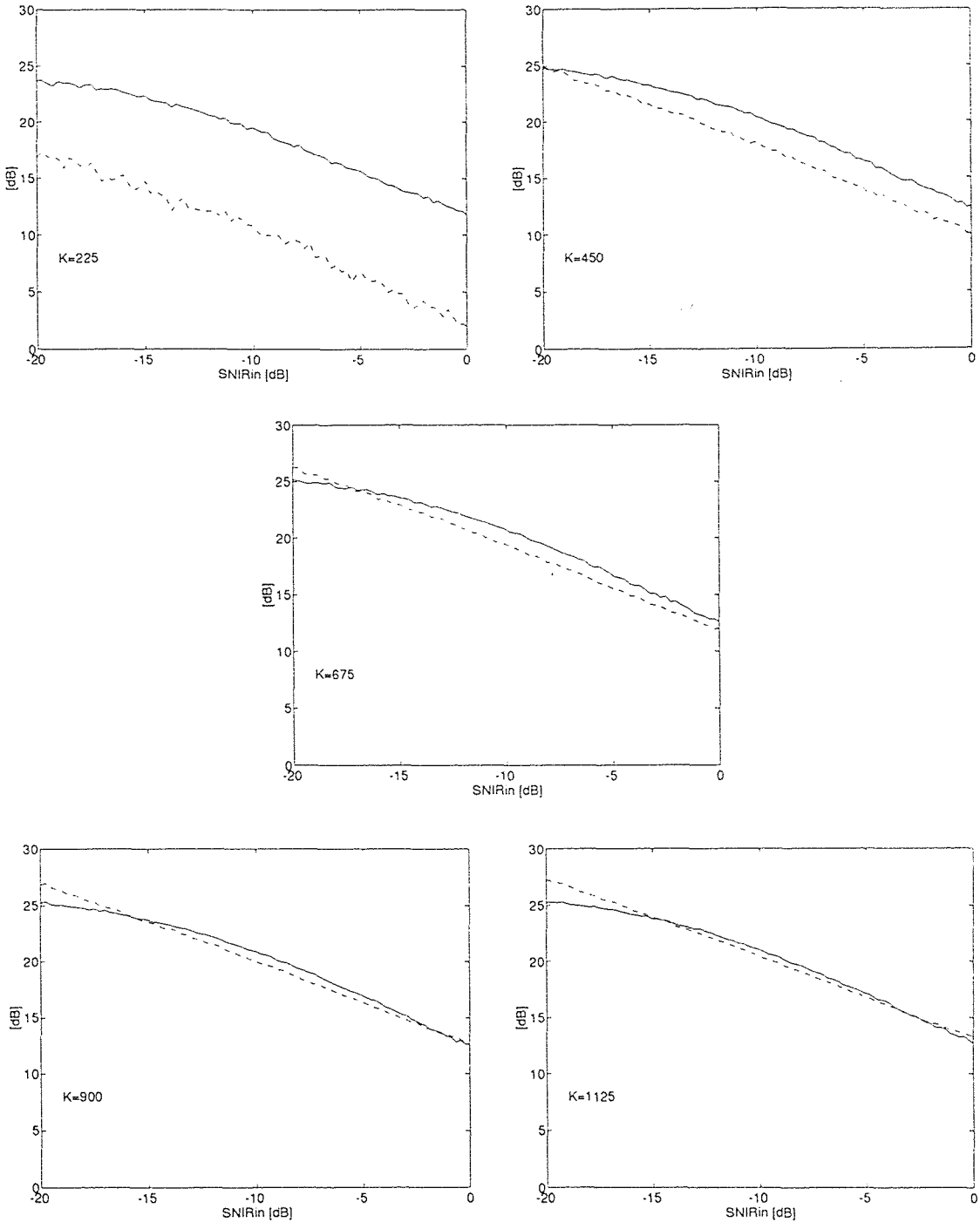

Figure 5.8 SNIR improvement factor vs. input SNIR for narrow-band interference [Solid] Eigencanceler [Dashed] Wiener-Hopf.

5.2.3 Probability of Error

The probability of error indicates the probability of recovering the desired signal. To simplify matters, in our simulations, only bits of value +1 are assumed to be sent. Therefore, any output of the filter which is negative is an error. The simulations are carried out on the Eigencanceler and the Wiener-Hopf, with SIR = -20 dB and SIR = -10 dB. The SNR is varied from -5 dB to 15 dB, and the probability of error is plotted against the SNR, accordingly. As a reference, the ideal BPSK is also plotted, to show the optimal probability of error at a given SNR.

Figure 5.9 depicts five plots of probability of error vs. SNR for different sizes of data blocks. At $K = 25$, given an SIR = -10 dB, the Eigencanceler consistently yields lower probability of error for each SNR than the Wiener-Hopf. The Wiener-Hopf yields a probability of error ranging from 1.2 to 16.5 times the probability of error yielded by the Eigencanceler. For an SIR = -20 dB, however, the performance of both systems is virtually identical throughout the SNR range. The similarity in the performances of both filters is consistent with SIR = -20 dB for all K. The difference in the performances of both filters is notable with SIR = -10 dB for $K = 25$ and $K = 50$. Above $K = 75$, the measurement noise pertubation has less of an effect on the Wiener-Hopf, thereby allowing it to yield a system performance comparable to that offered by the Eigencanceler. Once again, this indicates that given a few data, the Eigencanceler will offer a superior interference cancellation over the Wiener-Hopf.

The overall drop in probability of error for the Eigencanceler from $K = 25$ to $K = 125$ ranges from 1.05 to 31.8 for an SIR = -20 dB and from 1.01 to 29.8 for an SIR = -10 dB. The overall drop in probability of error for the Wiener-Hopf ranges from 1.09 to 17.7 for an SIR = -20 dB and from 1.36 to 257 for an SIR = -10 dB.

An analogous conclusion can be made to Figure 5.10 in that for SIR = -10 dB, the Wiener-Hopf begins with higher probability of error for $K = 225$ and lowers

the probability of error for values of K higher than 450, inclusive. However, the Eigencanceler yields probability of error at $K = 1125$ which ranges from 1 to 5.7516 times the probability of error at $K = 225$. Given an SIR = -20 dB, this factor ranges from 1.02 to 1.44, indicating that a five-fold increase in the size of the data block has little impact on the Eigencanceler, as opposed to the Wiener-Hopf.

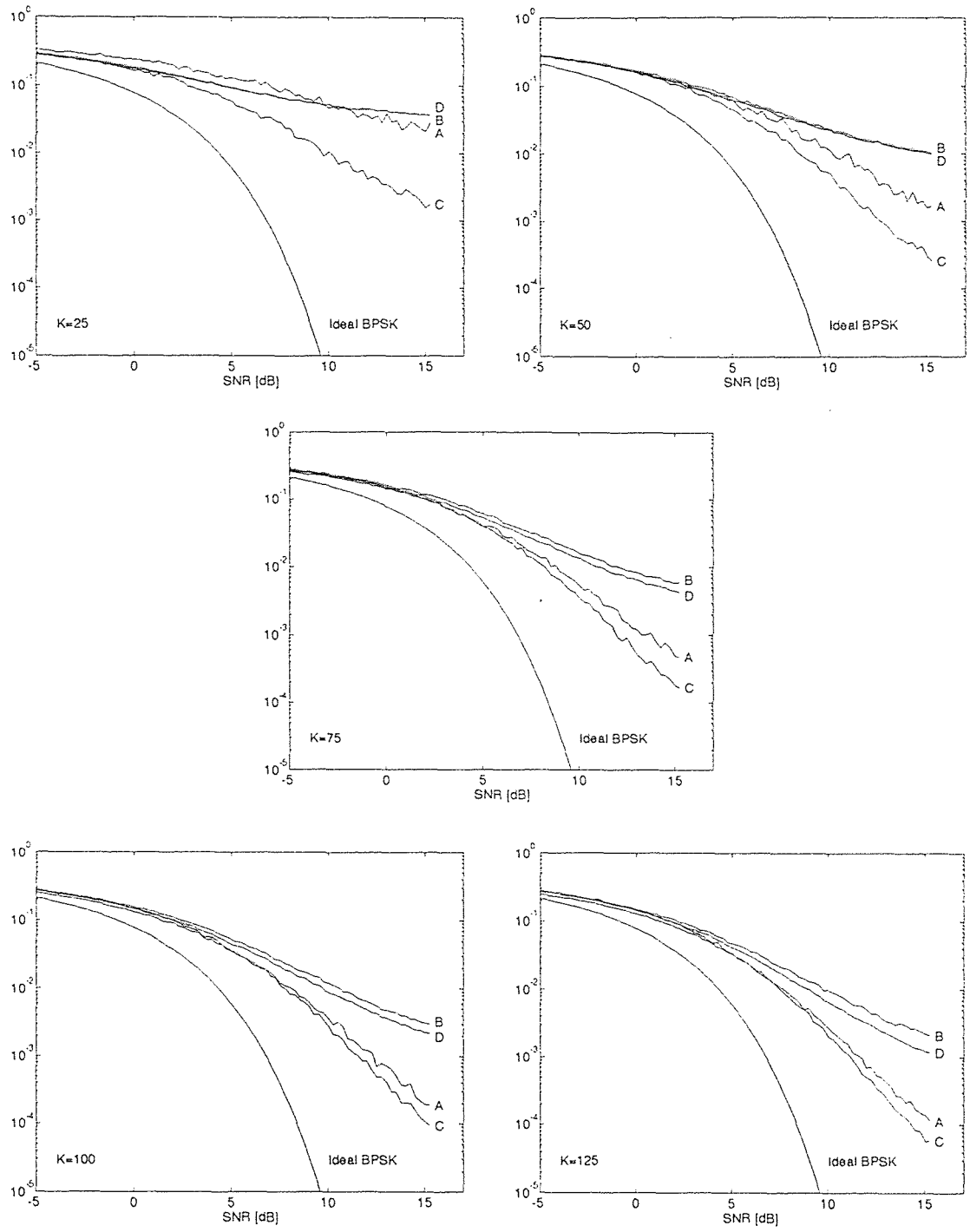

Figure 5.9 Probability of error vs. SNR for tone interference
[A]Wiener-Hopf (SIR = -10 dB) [B]Wiener-Hopf (SIR = -20 dB)
[C]Eigencanceler (SIR = -10 dB) [D]Eigencanceler (SIR = -20 dB).

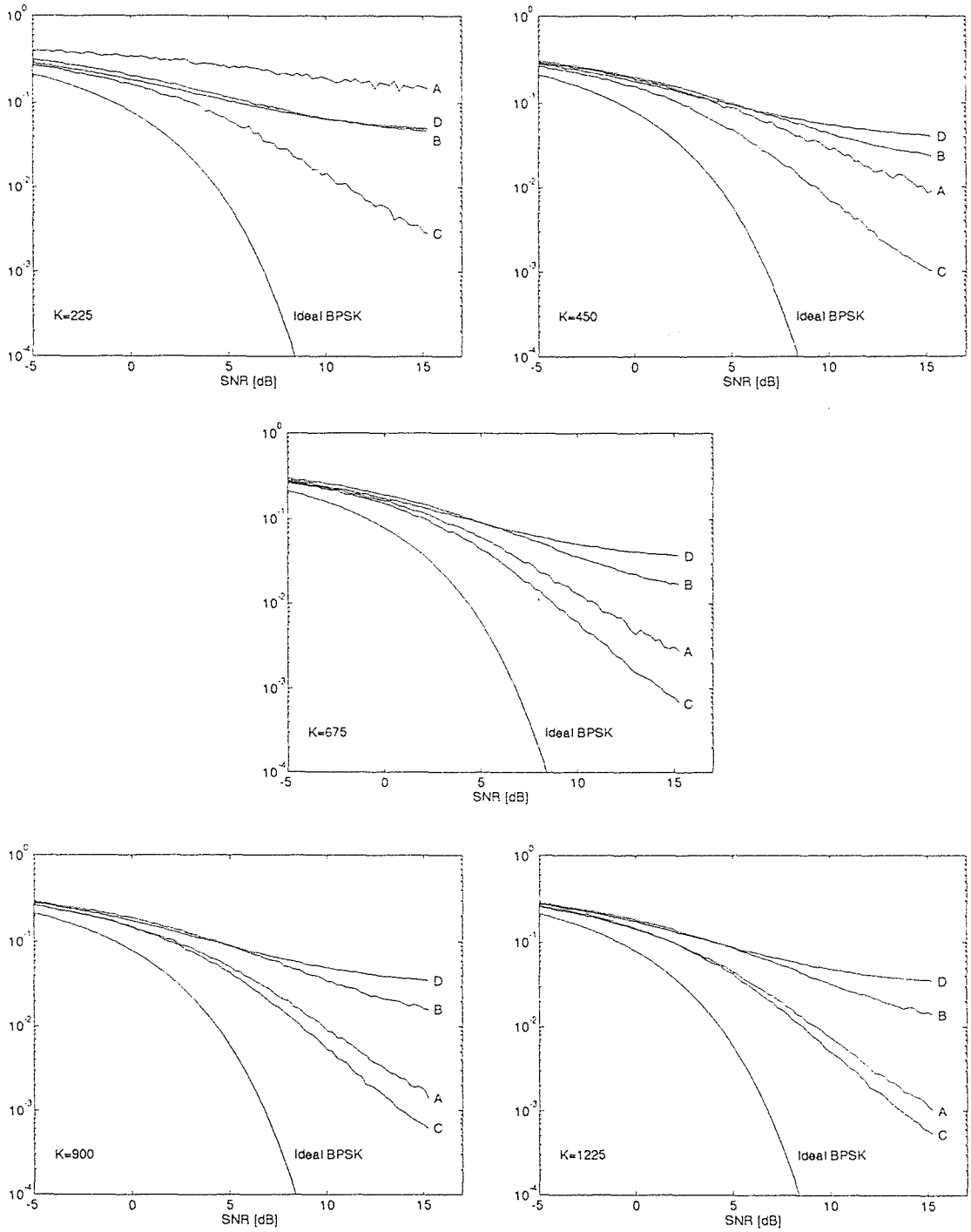

Figure 5.10 Probability of error vs. SNR for narrow-band interference
[A]Wiener-Hopf (SIR = -10 dB) [B]Wiener-Hopf (SIR = -20 dB)
[C]Eigencanceler (SIR = -10 dB) [D]Eigencanceler (SIR = -20 dB).

5.3 Performance of the Eigencanceler Algorithm vs. the LMS and the RLS

The Eigencanceler, the LMS, and the RLS algorithms are evaluated in the normalized variance of the weight vector, in the MS at the output of the filter, in the improvement of in SNIR η, and in the probability of error P_e. All evaluations are *learning curves* as they are plotted against time. Furthermore, 100 independent tests are run and Monte Carlo averaged for each plot. The algorithms are implemented in linear prediction error filters given a tone interference.

There are two sets of simulations for a tone interference, given an SIR = -10 dB and SIR = -20 dB. In order to evaluate the performance of the Eigencanceler in its robustness to the measurement noise, we use SNR = 10 dB, which is indicative of a reasonably strong presence of noise in the signal environment.

Figures 5.11-5.14 are plotted given an SIR = -10 dB. As the signal environment is stationary for our purposes, the forgetting factor γ used in the RLS algorithm is equal to unity. The small constant used to initialize the inverse of the correlation matrix $\mathbf{\Phi}$ is $\delta = 0.01$. The step-size in the LMS algorithm is $\mu = 0.001$.

Figure 5.11 illustrates the rapid convergence of the Eigencanceler algorithm to its optimal solution, in contrast to the LMS and the RLS. In the first iteration, the normalized variance of the Eigencanceler is 214.7153; however, rapid convergence takes place within the second iteration, where the variance is 0.0738. In contrast, the normalized variances of the RLS at the first and second iterations are 0.2975 and 0.2342, respectively. Likewise, the normalized variances of the LMS at the first and second iterations are 0.3043 and 0.2975, respectively. The similarity in the performances of the RLS and the LMS algorithms is attributed to a high noise environment, where SNR = 10 dB. It is well known that as the SNR increases, the RLS offers superior tracking performance to the LMS; however, in a low SNR environment, the two algorithms offer roughly the same performance.

Figure 5.12 depicts the MS at the output of the filter. After the initial spike in the MS at the output of the filter, the Eigencanceler rapidly converges to an MS of 4.5339 at the second iteration. Both the LMS and the RLS, to a lesser extent, fluctuate significantly until they converge at $k = 48$ and $k = 15$, respectively. Figures 5.13 and 5.14 show that the Eigencanceler consistently yields a lower probability of error, and correspondingly, a higher SNIR at the output of the filter until $k = 87$, at which point the RLS offers superior performance. The Eigencanceler offers an SNIR ranging from 5.8725 to 3.0155 [dB] over that offered by the RLS in the time range $k = 2$ to $k = 12$.

For the case where SIR = -20 dB, $\gamma = 1$, $\delta = 0.001$, and $\mu = 0.0001$. Figures 5.15-5.18 reflect the advantage the Eigencanceler takes of an increased eigenvalue spread, resulting from an increase in interference power given an SNR = 10 dB. Due to the increase in interference power by a factor of 10 dB, the eigenvalue spread is accordingly increased by a factor of 10 dB. Hence, the convergence rate of both the LMS and the RLS algorithms to the Wiener-Hopf solution and in the MS at the output of the filter is significantly decreased. Accordingly, the performances of the two algorithms in the probability of error and the SNIR at the output of the filter are adversely affected.

Figure 5.15 depicts the convergence of the algorithms in the normalized variance of their respective weight vectors. In the first iteration, the normalized variance of the Eigencanceler is 39.1061; however, rapid convergence takes place in the second iteration, where the variance is 0.0105. In contrast, the normalized variances of the RLS at the first and second iterations are 0.3184 and 0.2411, respectively. Furthermore, the normalized variances of the LMS at the first and second iterations are 0.3264 and 0.3169, respectively. Figure 5.12, depicting the MS at the output of the filter, reveals that the LMS and the RLS algorithms take longer to adapt to the signal environment in a highly negative SIR environment. In contrast, the MS at

the output of the Eigencanceler-based filter is 4.9861 at the second iteration, after the initial spike at the first iteration. Both the LMS and the RLS, to a lesser extent, fluctuate significantly until they converge at $k = 106$ and $k = 39$, respectively. Both the LMS and the RLS algorithms take roughly twice the amount of time to converge given SIR = -20 dB over SIR = -10 dB.

Figures 5.17 and 5.18 show that the Eigencanceler yields a lower probability of error, and correspondingly, a higher SNIR at the output of the filter until $k = 314$, at which point the RLS offers superior performance. The Eigencanceler offers an SNIR ranging from 15.6884 to 3.0435 [dB] over that offered by the RLS in the time range $k = 2$ to $k = 57$. Comparing these results to the ones obtained given SIR = -10 dB, we note that not only is *significantly superior* interference capability offered by the Eigencanceler, in contrast to the Wiener-based algorithms, the adaptation of the algorithm in a highly negative SIR environment is *faster* as well.

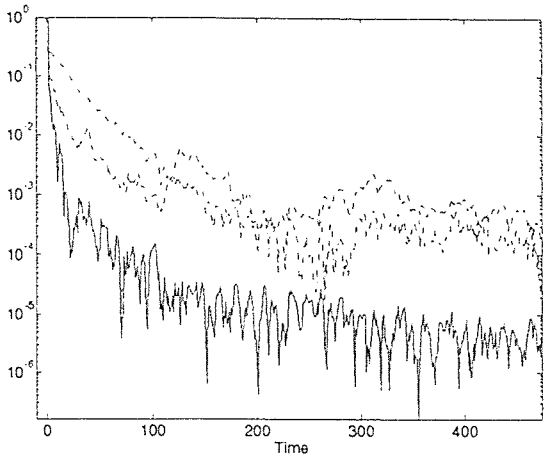

Figure 5.11 Normalized variance of the weight vectors.

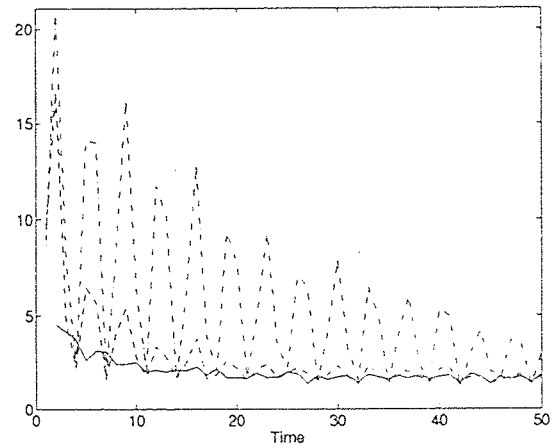

Figure 5.12 MS vs. time.

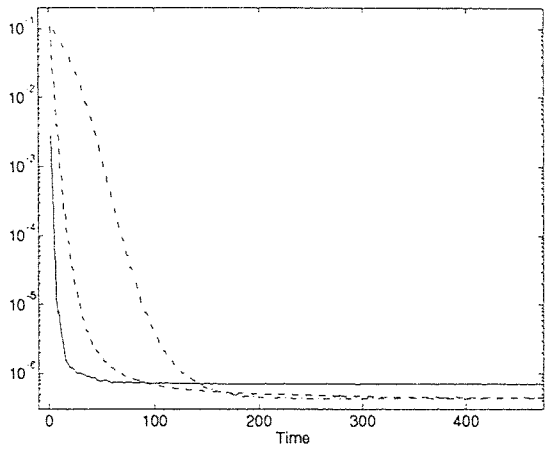

Figure 5.13 Probability of error vs. time.

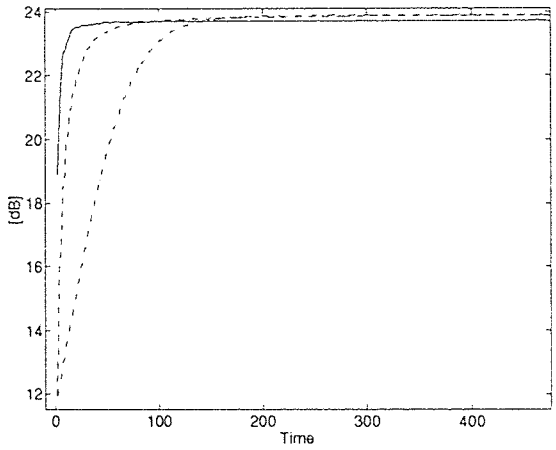

Figure 5.14 SNIR vs. time.

[Solid] Eigencanceler [Dashed] RLS [Dashed-Dotted] LMS
SIR = -10 dB SNR = 10 dB M = 5 L = 15

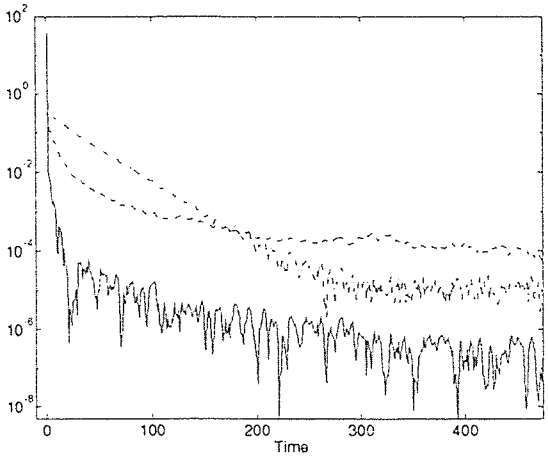

Figure 5.15 Normalized variance of the weight vectors.

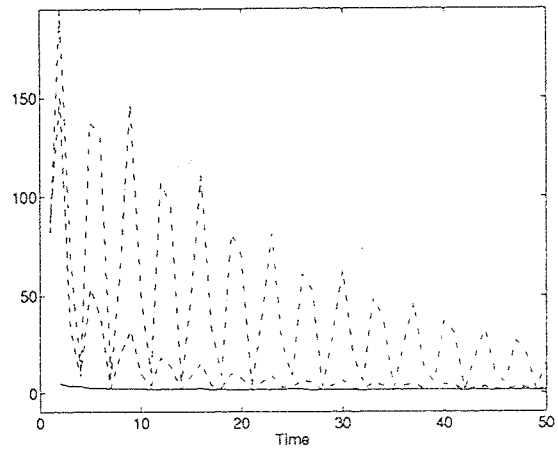

Figure 5.16 MS vs. time

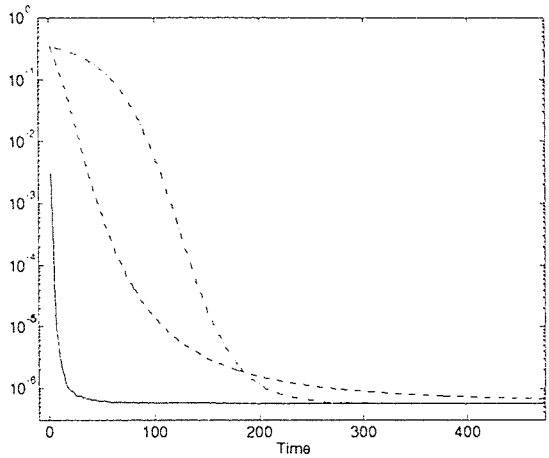

Figure 5.17 Probability of error vs. time.

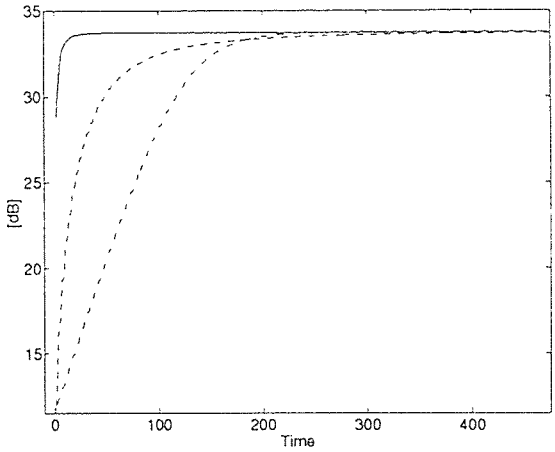

Figure 5.18 SNIR vs. time.

[Solid] Eigencanceler [Dashed] RLS [Dashed-Dotted] LMS
SIR = -20 dB SNR = 10 dB M = 5 L = 15

CHAPTER 6

CONCLUSIONS

A new approach to excising narrow-band interferences in spread spectrum systems was introduced in this work. The Eigencanceler exploits the eigen-properties of the received signal to separate the highly coherent interference from the relatively incoherent wide-band data. The following summarizes the evaluation of our method and algorithm:

- The Eigencanceler was shown to be more robust to measurement noise than the Wiener-based algorithms.
- Given few data in an *unknown* signal environment, the Eigencanceler method offers superior interference cancellation over the Wiener-Hopf filter.
- Likewise, the Eigencanceler algorithm proves to be fastly converging, especially in highly negative SIR environments, in contrast to the LMS and the RLS algorithms.
- The rapid convergence of the Eigencanceler algorithm is attributed to its robustness to measurement noise.
- The complexity of the Eigencanceler is on the order $\mathcal{O}(M^2)$.

REFERENCES

1. R. Compton, "An adaptive array in a spread-spectrum communication system," *Proc. IEEE*, vol. 66, no. 3, pp. 289–298, March 1978.

2. T. Durrani and K. Sharman, "Eigenfilter approaches to adaptive array processing," *Proc. IEE*, vol. 130, Pts. F and H, no. 1, pp. 22–28, February 1983.

3. E. Eleftheriou and D. Falconer, "Tracking properties and steady-state performance of RLS adaptive filter algorithms," *IEEE Trans. Acoustics, Speech, and Signal Processing*, vol. 34, no. 5, pp. 1097–1109, October 1986.

4. D. Godard, "Channel equalization using a Kalman filter for fast data transmission," *IBM J. Research and Development*, pp. 267–273, May 1974.

5. G. Golub and C. Van Loan, *Matrix Computations*, The John Hopkins University Press, Baltimore, Maryland, 1985.

6. A. Haimovich and Y. Bar-Ness, "An eigenanalysis interference canceller," *IEEE Trans. Signal Processing*, vol. 39, no. 1, pp. 76–84, January 1991.

7. A. Haimovich and A. Vadhri, "Rejection of narrow-band interferences in PN spread spectrum systems using an eigenanalysis algorithm," to be presented at *IEEE Statistical Signal Processing Workshop*, June 1994.

8. A. Haimovich and A. Vadhri, "Rejection of narrow-band interferences in PN spread spectrum sys tems using an eigenanalysis approach," to be presented at *Proc. IEEE Military Communications Conf.*, October 1994.

9. A. Haimovich and X. Wu, "Eigenanalysis based array processing for mobile communications," *Conf. Information Sciences and Systems*, vol. 28, March 1994.

10. S. Haykin, *Adaptive Filter Theory*, Prentice Hall, Englewood Cliffs, New Jersey, 2nd ed., 1991.

11. F. Hsu and A. Giordano, "Digital whitening techniques for improving spread spectrum communications performance in the presence of narrow-band jamming and interference," *IEEE Trans. Communications*, vol. 26, no. 2, pp. 209–216, February 1978.

12. R. Iltis and L. Milstein, "Performance analysis of narrow-band interference rejection techniques in DS spread-spectrum systems," *IEEE Trans. Communications*, vol. 32, no. 11, pp. 1169–1177, November 1984.

13. R. Iltis and L. Milstein, "An approximate statistical analysis of the Widrow LMS algorithm with application to narrow-band interference rejection," *IEEE Trans. Communications*, vol. 33, no. 2, pp. 121–130, February 1985.

14. J. Karhunen, "Adaptive algorithms for estimating eigenvectors of correlation type matrices," *Proc. IEEE Int. Conf. Acoustics, Speech, and Signal Processing*, 1984.

15. J. Ketchum and J. Proakis, "Adaptive algorithms for estimating and suppressing narrow-band interference in PN spread-spectrum systems," *IEEE Trans. Communications*, vol. 30, no. 5, pp. 913–923, May 1982.

16. L. Li and L. Milstein, "Rejection of narrow-band interference in PN spread-spectrum systems using transversal filters," *IEEE Trans. Communications*, vol. 30, no. 5, pp. 925–928, May 1982.

17. E. Masry, "Closed-form analytical results for the rejection of narrow-band interference in PN spread-spectrum systems - Part I: Linear prediction filters," *IEEE Trans. Communications*, vol. 33, no. 1, pp. 10–19, August 1984.

18. E. Masry, "Closed-form analytical results for the rejection of narrow-band interference in PN spread-spectrum systems - Part II: Linear interpolation filters," *IEEE Trans. Communications*, vol. 33, no. 1, pp. 10–19, January 1985.

19. L. Milstein, "Interference rejection techniques in spread spectrum communications," *Proc. IEEE*, vol. 76, no. 6, pp. 657–671, June 1988.

20. L. Milstein and R. Iltis, "Signal processing for interference rejection in spread spectrum communications," *IEEE ASSP Mag.*, pp. 14–31, April 1986.

21. R. Pickholtz, D. Schilling, and L. Milstein, "Theory of spread-spectrum communications - a tutorial," *IEEE Trans. Communications*, vol. 30, no. 5, pp. 855–884, May 1982.

22. G. Saulnier, P. Das, and L. Milstein, "An adaptive digital suppression filter for direct sequence spread spectrum communications," *IEEE J. Selected Areas in Communications*, vol. 3, no. 5, pp. 676–686, September 1985.

23. D. Slepian and H. Pollak, "Prolate spheroidal wave functions Fourier analysis and uncertainty - III: The dimension of the space of essentially time- and band-limited signals," *Bell System Tech. J.*, pp. 1295–1336, July 1990.

24. B. Widrow, P. Mantey, L. Griffiths, and B. Goode, "Adaptive antenna systems," *Proc. IEEE*, vol. 55, no. 12, pp. 2143–2158, December 1967.

25. B. Widrow, J. McCool, M. Larimore, and C. Johnson, "Stationary and nonstationary learning characteristics of the LMS adaptive filter," *Proc. IEEE*, vol. 64, no. 8, pp. 1151–1162, August 1976.